



Optimized fuzzy self-tuning PID controller design based on Tribe-DE optimization algorithm and rule weight adjustment method for load frequency control of interconnected multi-area power systems

Neda Jalali, Hadi Razmi ^{*}, Hasan Doagou-Mojarrad

Department of Electrical Engineering, East Tehran Branch, Islamic Azad University, Tehran, Iran



ARTICLE INFO

Article history:

Received 10 September 2019
Received in revised form 18 March 2020
Accepted 16 May 2020
Available online 26 May 2020

Keywords:

Fuzzy self-tuning PID controller
Load frequency control
Rule weight adjustment method
Tribe-DE optimization algorithm

ABSTRACT

The reliable load frequency control (LFC) is addressed as one of the most important services in the modern electric power system operation and planning. Since the power systems have various structural and non-structural uncertainties, using control methods with fixed parameters may not yield the optimal performance of the system. Thus, in this research, a novel fuzzy PID controller is introduced to LFC for interconnected multi-area power systems in parametric uncertainties as well as external disturbances existence. The proposed algorithm adjusts the scaling factors and the modal parameters of input and output membership functions as well as the weights of fuzzy PID controller rule values. According to the transient response of the area control error (ACE) variable partitioning, the fuzzy rule weight values are obtained. Furthermore, in order to enhance the quality of the response, the scaling factors and the modal parameters of the input and output membership functions of fuzzy PID controllers are optimized by Tribe-DE (TDE) algorithm. The method is examined on the two and three area interconnected power systems at several conditions and an Integral of Time multiplied Absolute Error (ITAE) less than 0.0108 as well as an absolute maximum undershoot less than 0.0210 Hz for Δf_1 regulation are obtained in the two area interconnected power system. Good transient behavior, disturbance rejection capability and insensitivity to parameter changes are advantages of the proposed controller.

© 2020 Elsevier B.V. All rights reserved.

1. Introduction

Deviations in scheduled power interchanges with interconnected control areas and system frequency during generation-load mismatches have been recognized as one of the major threats to multi-area large scale power systems [1]. Secondary frequency control, which is called automatic generation control and/or load frequency control, plays the key role in designing and operating power systems in order to provide adequate and reliable electric power possessing good quality [2] and its design has become a major challenge for academic and industry researchers. A well-designed load frequency controller should have some advantages as follows [3]: (1) presenting good steady state and transient responses, (2) disturbance rejection capability, (3) insensitivity to parameter variations, and (4) significant stability as well as performance robustness. So far, different approaches have been suggested for LFC in the literature, such as adaptive

control, optimal control, intelligent control and robust control techniques [1,4]. PI and PID controllers are the most well-known approaches used to LFC issue [5]. In terms of PI/PID gains selection methods, these types of controllers can be divided into two main categories: Adaptive and non-adaptive controllers [6]. In non-adaptive controllers, adjusted gains remain fixed during the operation. Several optimization methods such as differential evolution algorithm [7], bacteria foraging optimization algorithm [8], firefly algorithm [9], multi-objective uniform diversity genetic algorithm [5], teaching learning based optimization algorithm [10], quasi-oppositional harmony search algorithm [11,12], and hybrid harmony search and cuckoo optimization algorithm [13] are the most well-known methods for PI/PID gains selection applied to LFC in recent years.

Conventional non-adaptive PID controllers have linear structure and are designed at specific operating condition, however, because of the presence of nonlinearities in real systems, the controlled system may no longer be suitable in all operating points; thus, the performance of conventional PI/PID controllers are required to be improved [14]. In order to overcome this drawback, fuzzy logic can be regarded as one of the most efficient methods applied to PI/PID controller design in the literature. Applying

* Corresponding author.

E-mail addresses: nedajalali306@gmail.com (N. Jalali), razmi.hadi@gmail.com (H. Razmi), [\(H. Doagou-Mojarrad\).](mailto:hasan_doagou@yahoo.com)

Nomenclature

DE	Differential Evolution
2DOF	Two Degree of Freedom
IDD	Integral plus Double Derivative
NR	Not Reported
NaN	Not a Number
GRC	Generation Rate Constraint
TDE	Tribe-DE
HVDC	High Voltage Direct Current
LFC	Load Frequency Control
AGC	Automatic Generation Control
PI	Proportional-Integral
PD	Proportional-Derivative
PID	Proportional-Integral-Derivative
ACE	Area Control Error
FLC	Fuzzy Logic Controller
COG	Center of Gravity
MF	Membership Function
ITAE	Integral of Time multiplied Absolute Error
HSCOA	Harmony Search Cuckoo Optimization Algorithm
SLP	Step Load Perturbation
BFOA	Bacterial Foraging Optimization Algorithm
hPSO-PS	Hybrid Particle Swarm Optimization and Pattern Search
ind_m	The solution vector of the individual m
ind_m^{\max}	The maximum value of ind_m
ind_m^{\min}	The minimum value of ind_m
rand	The random real number
rand	The random real vector
N_{itr}	Number of iterations
N_{ind}	Number of individuals
N_{trb}	Number of tribes
μ	The mutation parameter
c_p	The probability of crossover
Δf_i	Frequency deviation in the control area i (Hz)
$T_{GT,i}^{(k)}$	Speed governor time constant of the k th thermal unit in the control area i (s)
$T_{TT,i}^{(k)}$	Time constant of the k th steam turbine in the control area i (s)
$T_{RT,i}^{(k)}$	Reheat time constant of the k th thermal unit in the control area i (s)
$K_{RT,i}^{(k)}$	Reheat coefficient of the k th thermal unit in the control area i
$K_{T,i}^{(k)}$	Participation factor of the k th thermal unit in the control area i
$R_{T,i}^{(k)}$	Speed regulation constant of the k th thermal unit in the control area i (Hz/p.u.)
$T_{GH,i}^{(k)}$	Time constant of the k th hydro turbine speed governor in the control area i (s)

subgroup, there are no explicit PI/PID gains; instead the control signal or the incremental change of the control signal is directly derived from the fuzzy inference and the knowledge basis. In the second subgroup, the gains of the PI/PID controller are adjusted on-line, and then the control signal or the incremental change of the control signal is produced by the conventional PI/PID controller.

Furthermore, the fuzzy logic design parameters are divided into two general categories [16]: (1) structural parameters including fuzzy rules, input/output variables to fuzzy inference, membership functions, fuzzy linguistic sets, inference mechanism and defuzzification method, and (2) tuning parameters including parameters of membership functions, input/output scaling factors, the ultimate gain and the ultimate period of the controlled system as well as the initial value of proportional, integral and derivative gains.

Literature survey in the field of LFC reveals that most of the application of fuzzy logic to PI/PID controller design belongs to the first subgroup; i.e. fuzzy PID controllers.

In [13], a hybrid algorithm is proposed to design a fuzzy PI/PID controller for LFC in a multi-area power system. In the paper, the scaling factors of fuzzy PI/PID controllers for a two-area thermal power system are defined with the evolutionary algorithm. In this regard, the proposed method feasibility is established under varying loading conditions and system parameters. Also, a fuzzy PI/PID controller based on bacterial foraging optimization algorithm is proposed in [17] for AGC of traditional/restructured multi-area interconnected power systems. The simulation results in terms of IAE, ITAE, ISE and ITSE, peak undershoots and settling times of tie-line and frequency responses have been reported. In [18], a nonlinear fuzzy PID controller coordinated with Thyristor Controlled Series Compensator (TCSC) is suggested for LFC problem using novel Modified Differential Evolution (MDE) algorithm. Moreover, in [19], a Fractional Order PID (FOPID) controller is presented considering governor saturation for load frequency control based on Gases Brownian Motion Optimization (GBMO). The performance of proposed algorithm is robust against parameters changes. In [20], the fuzzy PID controller scaling factors are obtained using a novel hybrid Teaching Learning Based Optimization (TLBO) and Local Unimodal Sampling (LUS). It was clear from the results that the suggested hybrid approach can obtain higher quality solution regarding to the conventional PID controllers. Also, a fuzzy PI controller for AGC is presented in [21] based on novel hybrid Pattern Search (PS) and Particle Swarm Optimization (PSO). The results obtained from the proposed method are compared with those of the other methods such as Genetic Algorithm (GA), DE, conventional Ziegler Nichols (ZN), BFOA as well as hybrid BFOA-PSO. The suggested fuzzy PI controller is robust against the changes in system parameters and loading conditions. In [22], to tune the scaling factors of fuzzy PID controller with triangular membership function, spider monkey optimization (SMO) is used. The suggested algorithm is examined on a two-area interconnected thermal power system.

It is found that two problems arise when the fuzzy PI/PID controller is used: firstly, how to choose the optimal gains of the PI/PID controller, and secondly, how to set the best design parameters of the fuzzy logic, in order to improve its efficiency. These two problems are crucial because the optimal gains of the PI/PID controller choice influence the appropriate design parameters of the fuzzy logic and vice versa. Therefore, obtaining the optimal gains of the PI/PID controller and the design parameters of the fuzzy logic must occur simultaneously. In the literature, fuzzy logic has been used for selection of the optimal PI/PID gains. However, the aforementioned papers focused on optimal PI/PID gains selection and did not deal with the selection of design

fuzzy logic to PI/PID controller design is generally categorized into two main subgroups considering their construction [15]: (1) fuzzy PI/PID controllers, and (2) fuzzy PI/PID-like controllers. In the first

parameters for the fuzzy logic. Usually these parameters are off-line chosen by the trial and error method and remain unchanged during the operation.

Due to parameter uncertainties and external disturbances in the real systems, the application of fixed design parameters may not result in optimal system performance. Therefore, in order to overcome this drawback, a new fuzzy PID controller has been suggested in this paper for the LFC of interconnected multi-area power systems in the presence of parametric uncertainties and load disturbances. The proposed method adjusts the fuzzy rule weights, as well as, PID gains of the fuzzy PID controller. In addition, the optimal values of some design parameters of the fuzzy PID controller are determined by an optimization method. DE is a direct search optimization algorithm that is able to handle a variety of objective functions. One of the main challenges in the conventional DE is preventing the algorithm from getting stuck in local optimum of the objective function because of the loss of population diversity [23]. In the current research, the Tribe-DE (TDE) algorithm is proposed to prevent this prematurity. In this model, population is divided into three stages, and individuals are controlled at each stage to maintain population diversities. The modal parameters of the input and output membership functions and the scaling factors of fuzzy PID controllers are optimized by TDE algorithm. Moreover, in this paper, the step response of the fuzzy PID controller structure is divided into four main areas and an on-line weight tuning approach is suggested. This method was first proposed in reference [24] and is used here to solve the load-frequency control problem. The rule weight value settings are arranged directly based on the area control error absolute value function as the weight values. The rule weight defines the importance of a fuzzy rule for the inputs. The implementation of this method increases the controller's robustness against different uncertainties. Correspondingly, the results of simulation are exhibited to show the efficiency of the proposed method in comparison to the other methods in various cases of multi-area interconnected power systems. It should be noted that one of the challenges of using the on-line method proposed in this paper is the computational complexity of the method compared to the case of not using it. However, given the recent advances in speeding up the computation, this challenge is not a major drawback and therefore has not been addressed in this article.

Table 1 shows the comparison of selection methods of the fuzzy PI/PID controller design parameters investigated in this paper with other similar published papers.

The aims of this research are reducing sensitivity to parametric uncertainties and external disturbances, improving the quality of the response in terms of ITAE, settling time, maximum overshoot as well as absolute maximum undershoot. It also aimed to compare the performances of the proposed fuzzy PID controller method with similar recently published approaches for a two area non-reheat thermal interconnected power system, a multi-source two area power system with/without HVDC link and a three area reheat thermal interconnected nonlinear power system in different cases with varying loading conditions and system parameters.

The contributions of the paper can be summarized as follows:

- The TDE optimization algorithm is used for the optimal selecting of input-output scaling factors and MF parameters of fuzzy PID controllers in order to improve the quality of the response. The proposed evolutionary algorithm prevents the occurrence of the early convergence by increasing the population diversity;
- An error-based on-line rule weight adjustment method is considered for fuzzy PID controllers, ensuring less sensitivity to various structural and non-structural uncertainties (main contribution); and

- Through combining the rule weight adjustment method with TDE optimization algorithm, better results are obtained in regulation performance in comparison to the results reported in the references [13,17] and [21], regarding ITAE, settling time, and absolute maximum undershoot.

The layout of the paper is organized as follows:

The dynamic models of power system components are described in Section 2. Section 3 describes the problem statement. The controller design and a brief overview of the proposed TDE algorithm are introduced in Section 4. The simulations results and discussion are given in Section 5. Finally, Section 6 concludes the paper.

2. System description

Since in the case of the LFC, the power system taken into consideration is subjected to small load disturbances, the effect of fast transients can be ignored and the linear models that consider the relatively slow dynamics of the turbine governors have been implemented to study and analyze the LFC issue [25,26]. A large-scale multi-area interconnected power system consisting of n control areas with mixed type of power generations connected by AC-DC tie-lines is considered here. The block diagram of the i th control area is shown in Fig. 1. Due to economic and technical considerations, thermal, hydro and gas units have been selected for the LFC commitment [27]. As can be seen in Fig. 1, the number of thermal, hydro and gas units in the i th control area is considered to be p , q and r , respectively. These power plants contain two main parts: speed governing subsystem as well as turbine subsystem. Fig. 2 shows the block diagram of the turbine governors of the k th thermal, hydro and gas units in the control area i . In this figure, the effects of governor dead band and generation rate constraint have been ignored. In addition to turbine governor dynamics, the LFC model shown in Fig. 1 also includes the dynamics of the electrical subsystem and the AC-DC tie-lines interchange, and the droop characteristics. The mathematical equations of each element in the i th control area are given in the following subsections [13].

2.1. Thermal units

As shown in Fig. 2-(a), mathematical equations of the k th thermal unit in the control area i can be obtained directly from the block diagram as follows:

- For reheat thermal units:

$$\dot{x}_{1T,i}^{(k)} = -\frac{1}{T_{GT,i}^{(k)}}x_{1T,i}^{(k)} - \frac{1}{R_{T,i}^{(k)}T_{GT,i}^{(k)}}\Delta f_i + \frac{1}{T_{GT,i}^{(k)}}u_{T,i}^{(k)} \quad (1)$$

$$\dot{x}_{2T,i}^{(k)} = \frac{T_{GT,i}^{(k)} - K_{RT,i}^{(k)}}{T_{RT,i}^{(k)}T_{GT,i}^{(k)}}x_{1T,i}^{(k)} - \frac{1}{T_{RT,i}^{(k)}}x_{2T,i}^{(k)} - \frac{K_{RT,i}^{(k)}}{R_{T,i}^{(k)}T_{GT,i}^{(k)}}\Delta f_i + \frac{K_{RT,i}^{(k)}}{T_{GT,i}^{(k)}}u_{T,i}^{(k)} \quad (2)$$

$$\dot{x}_{3T,i}^{(k)} = \frac{K_{T,i}^{(k)}}{T_{TT,i}^{(k)}}x_{2T,i}^{(k)} - \frac{1}{T_{TT,i}^{(k)}}x_{3T,i}^{(k)} \quad (3)$$

- For non-reheat thermal units:

$$\dot{x}_{1T,i}^{(k)} = -\frac{1}{T_{GT,i}^{(k)}}x_{1T,i}^{(k)} - \frac{1}{R_{T,i}^{(k)}T_{GT,i}^{(k)}}\Delta f_i + \frac{1}{T_{GT,i}^{(k)}}u_{T,i}^{(k)} \quad (4)$$

$$\dot{x}_{3T,i}^{(k)} = \frac{K_{T,i}^{(k)}}{T_{TT,i}^{(k)}}x_{1T,i}^{(k)} - \frac{1}{T_{TT,i}^{(k)}}x_{3T,i}^{(k)} \quad (5)$$

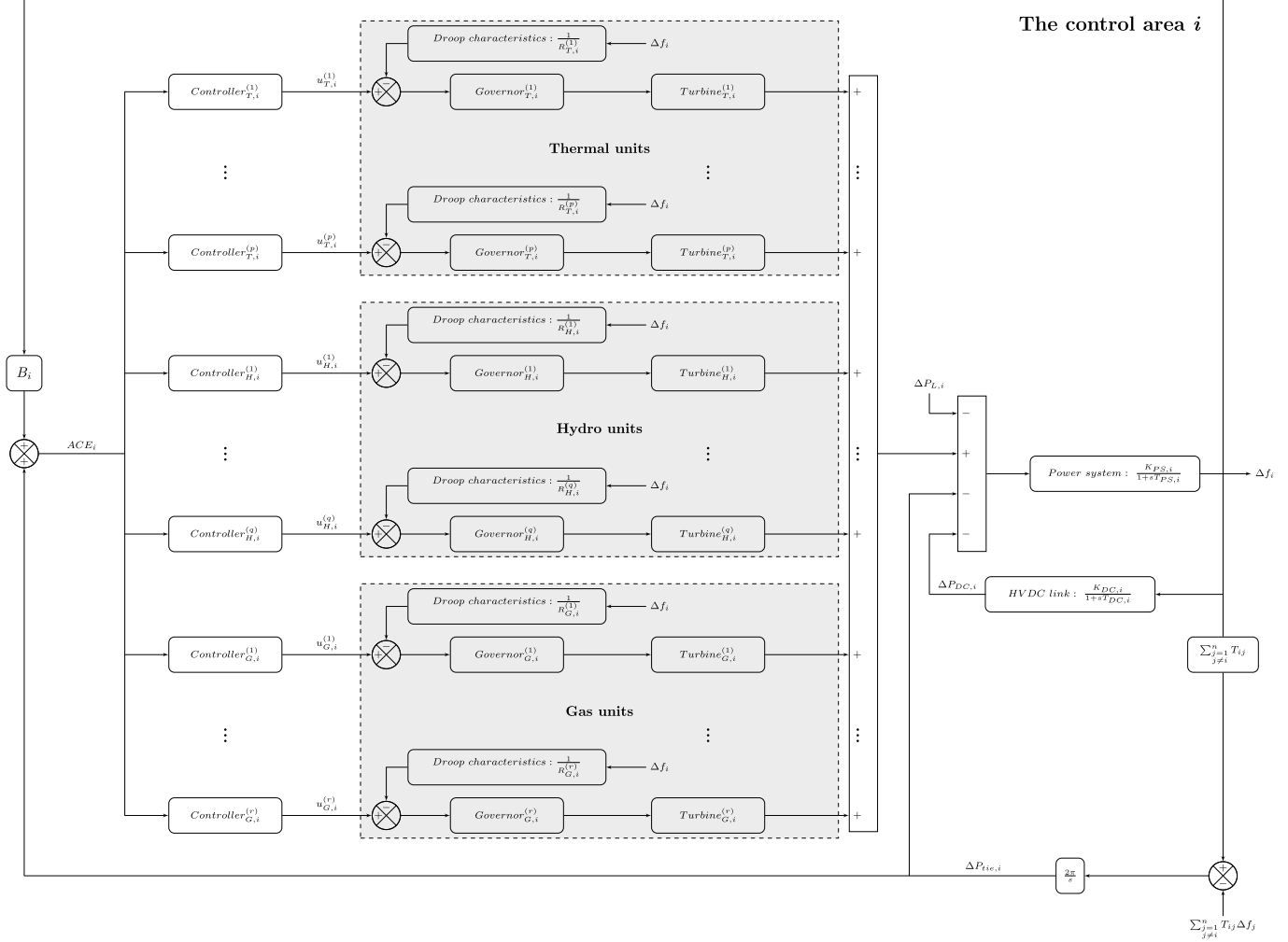


Fig. 1. The block diagram of the control area i .

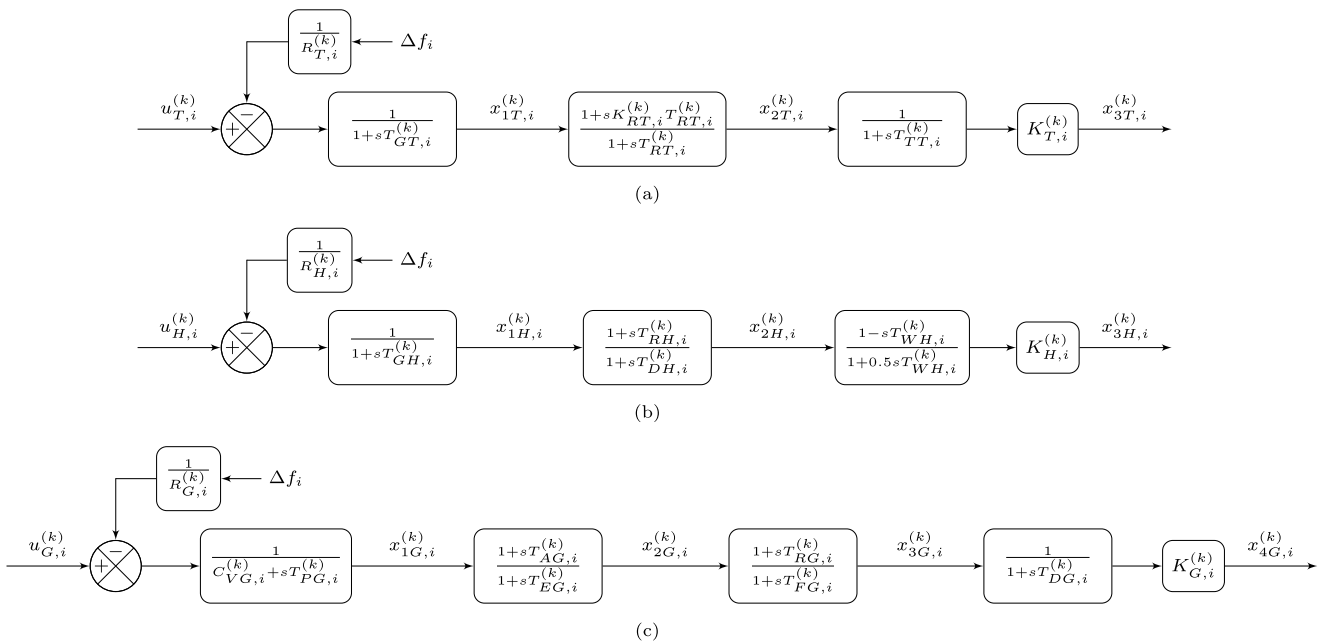


Fig. 2. The block diagram of (a) the k th thermal unit, (b) the k th hydro unit and (c) the k th gas unit in the control area i .

Table 1

Comparison of the selection methods of the fuzzy PI/PID controller design parameters.

	Input-output scaling factors	Modal parameters of MFs	Weights of fuzzy rules	Other structural and tuning parameters
[13]	HSCOA method (off-line)	The trail and error method (off-line)	The trail and error method (off-line)	The trail and error method (off-line)
[17]	BFOA method (off-line)	The trail and error method (off-line)	The trail and error method (off-line)	The trail and error method (off-line)
[21]	hPSO-PS method (off-line)	The trail and error method (off-line)	The trail and error method (off-line)	The trail and error method (off-line)
Proposed method	TDE method (off-line)	TDE method (off-line)	An error-based adjustment method (on-line)	The trail and error method (off-line)

2.2. Hydro units

From Fig. 2-(b), dynamic equations for the k th hydro unit in the control area i can be expressed as:

$$\dot{x}_{1H,i}^{(k)} = -\frac{1}{T_{GH,i}^{(k)}}x_{1H,i}^{(k)} - \frac{1}{R_{H,i}^{(k)}T_{GH,i}^{(k)}}\Delta f_i + \frac{1}{T_{GH,i}^{(k)}}u_{H,i}^{(k)} \quad (6)$$

$$\begin{aligned} \dot{x}_{2H,i}^{(k)} &= \frac{T_{GH,i}^{(k)} - T_{RH,i}^{(k)}}{T_{DH,i}^{(k)}T_{GH,i}^{(k)}}x_{1H,i}^{(k)} - \frac{1}{T_{DH,i}^{(k)}}x_{2H,i}^{(k)} - \frac{T_{RH,i}^{(k)}}{R_{H,i}^{(k)}T_{DH,i}^{(k)}T_{GH,i}^{(k)}}\Delta f_i \\ &\quad + \frac{T_{RH,i}^{(k)}}{T_{DH,i}^{(k)}T_{GH,i}^{(k)}}u_{H,i}^{(k)} \end{aligned} \quad (7)$$

$$\begin{aligned} \dot{x}_{3H,i}^{(k)} &= \frac{2K_{H,i}^{(k)}T_{RH,i}^{(k)} - 2K_{H,i}^{(k)}T_{GH,i}^{(k)}}{T_{DH,i}^{(k)}T_{GH,i}^{(k)}}x_{1H,i}^{(k)} + \frac{2K_{H,i}^{(k)}T_{DH,i}^{(k)} - 2K_{H,i}^{(k)}T_{WH,i}^{(k)}}{T_{DH,i}^{(k)}T_{WH,i}^{(k)}}x_{2H,i}^{(k)} \\ &\quad + \frac{2K_{H,i}^{(k)}T_{RH,i}^{(k)}}{R_{H,i}^{(k)}T_{DH,i}^{(k)}T_{GH,i}^{(k)}}\Delta f_i - \frac{2K_{H,i}^{(k)}T_{RH,i}^{(k)}}{T_{DH,i}^{(k)}T_{GH,i}^{(k)}}u_{H,i}^{(k)} \end{aligned} \quad (8)$$

2.3. Gas units

Differential equations for the k th gas unit in the control area i can be deduced directly from Fig. 2-(c):

$$\dot{x}_{1G,i}^{(k)} = -\frac{C_{VG,i}^{(k)}}{T_{PG,i}^{(k)}}x_{1G,i}^{(k)} - \frac{1}{R_{G,i}^{(k)}T_{PG,i}^{(k)}}\Delta f_i + \frac{1}{T_{PG,i}^{(k)}}u_{G,i}^{(k)} \quad (9)$$

$$\begin{aligned} \dot{x}_{2G,i}^{(k)} &= \frac{T_{PG,i}^{(k)} - T_{AG,i}^{(k)}C_{VG,i}^{(k)}}{T_{EG,i}^{(k)}T_{PG,i}^{(k)}}x_{1G,i}^{(k)} - \frac{1}{T_{EG,i}^{(k)}}x_{2G,i}^{(k)} - \frac{T_{AG,i}^{(k)}}{R_{G,i}^{(k)}T_{EG,i}^{(k)}T_{PG,i}^{(k)}}\Delta f_i \\ &\quad + \frac{T_{AG,i}^{(k)}}{T_{EG,i}^{(k)}T_{PG,i}^{(k)}}u_{G,i}^{(k)} \end{aligned} \quad (10)$$

$$\begin{aligned} \dot{x}_{3G,i}^{(k)} &= \frac{T_{PG,i}^{(k)}T_{RG,i}^{(k)} - T_{AG,i}^{(k)}C_{VG,i}^{(k)}T_{RG,i}^{(k)}}{T_{EG,i}^{(k)}T_{PG,i}^{(k)}T_{FG,i}^{(k)}}x_{1G,i}^{(k)} - \frac{T_{EG,i}^{(k)} + T_{RG,i}^{(k)}}{T_{EG,i}^{(k)}T_{FG,i}^{(k)}}x_{2G,i}^{(k)} \\ &\quad - \frac{1}{T_{FG,i}^{(k)}}x_{3G,i}^{(k)} - \frac{T_{AG,i}^{(k)}T_{RG,i}^{(k)}}{R_{G,i}^{(k)}T_{EG,i}^{(k)}T_{PG,i}^{(k)}T_{FG,i}^{(k)}}\Delta f_i + \frac{T_{AG,i}^{(k)}T_{RG,i}^{(k)}}{T_{EG,i}^{(k)}T_{PG,i}^{(k)}T_{FG,i}^{(k)}}u_{G,i}^{(k)} \end{aligned} \quad (11)$$

$$\dot{x}_{4G,i}^{(k)} = \frac{K_{G,i}^{(k)}}{T_{DG,i}^{(k)}}x_{3G,i}^{(k)} - \frac{1}{T_{DG,i}^{(k)}}x_{4G,i}^{(k)} \quad (12)$$

2.4. The electrical subsystem

According to the block diagram in Fig. 1, the mathematical description of the electrical subsystem in the control area i can be obtained as:

$$\dot{\Delta f}_i = \frac{K_{PS,i}}{T_{PS,i}}\Delta P_{G,i} - \frac{1}{T_{PS,i}}\Delta f_i - \frac{K_{PS,i}}{T_{PS,i}}\Delta P_{tie,i} - \frac{K_{PS,i}}{T_{PS,i}}\Delta P_{DC,i} - \frac{K_{PS,i}}{T_{PS,i}}\Delta P_{L,i} \quad (13)$$

Where, $\Delta P_{G,i} = \sum_{k=1}^p [x_{1T,i}^{(k)} + x_{2T,i}^{(k)} + x_{3T,i}^{(k)}] + \sum_{k=1}^q [x_{1H,i}^{(k)} + x_{2H,i}^{(k)} + x_{3H,i}^{(k)}] + \sum_{k=1}^r [x_{1G,i}^{(k)} + x_{2G,i}^{(k)} + x_{3G,i}^{(k)} + x_{4G,i}^{(k)}]$.

Also, the total AC tie-line power change between the area i and the other areas can be calculated as:

$$\dot{\Delta P}_{tie,i} = 2\pi \sum_{\substack{j=1 \\ j \neq i}}^n T_{ij}(\Delta f_j - \Delta f_i) \quad (14)$$

And, a simplified dynamic equation for the HVDC link in the control area i can be expressed as:

$$\dot{\Delta P}_{DC,i} = -\frac{1}{T_{DC,i}}\Delta P_{DC,i} + \frac{K_{DC,i}}{T_{DC,i}}\Delta f_i \quad (15)$$

2.5. The area control error (ACE)

The ACE for each area is a linear combination of the local frequency deviation and the tie-line AC power flow. For the control area i , the ACE can be deduced directly from Fig. 1:

$$ACE_i = B_i\Delta f_i + \Delta P_{tie,i} \quad (16)$$

3. Problem statement

According to Eqs. (1) to (16), LFC model differential equations can be shown as the compact state space form as follows:

$$\begin{cases} \dot{\mathbf{x}} = \mathbf{Ax} + \mathbf{Bu} + \mathbf{Dw} \\ \mathbf{y} = \mathbf{Cx} \end{cases} \quad (17)$$

Where, $\mathbf{x}^T = [x_1^T, \dots, x_n^T]$ is the system state vector, $\mathbf{u}^T = [u_1^T, \dots, u_n^T]$ is the control input vector, $\mathbf{y}^T = [ACE_1, \dots, ACE_n]$ is the output vector and $\mathbf{w}^T = [\Delta P_{L,1}, \dots, \Delta P_{L,n}]$ is the disturbance input vector. Also,

$$\mathbf{x}_i^T = [x_{1T,i}^T, x_{2T,i}^T, x_{3T,i}^T, \Delta f_i, \Delta P_{tie,i}, \Delta P_{DC,i}] \quad (18)$$

$$\mathbf{u}_i^T = [u_{1T,i}^T, u_{2T,i}^T, u_{3T,i}^T] \quad (19)$$

Where,

$$\mathbf{x}_{T,i}^T = [x_{1T,i}^{(1)}, \dots, x_{1T,i}^{(p)}, x_{2T,i}^{(1)}, \dots, x_{2T,i}^{(p)}, x_{3T,i}^{(1)}, \dots, x_{3T,i}^{(p)}] \quad (20)$$

$$\mathbf{x}_{H,i}^T = [x_{1H,i}^{(1)}, \dots, x_{1H,i}^{(q)}, x_{2H,i}^{(1)}, \dots, x_{2H,i}^{(q)}, x_{3H,i}^{(1)}, \dots, x_{3H,i}^{(q)}] \quad (21)$$

$$\begin{aligned} \mathbf{x}_{G,i}^T &= [x_{1G,i}^{(1)}, \dots, x_{1G,i}^{(r)}, x_{2G,i}^{(1)}, \dots, x_{2G,i}^{(r)}, x_{3G,i}^{(1)}, \dots, x_{3G,i}^{(r)}, \\ &\quad x_{4G,i}^{(1)}, \dots, x_{4G,i}^{(r)}] \end{aligned} \quad (22)$$

$$\mathbf{u}_{T,i}^T = [u_{1T,i}^{(1)}, \dots, u_{1T,i}^{(p)}] \quad (23)$$

$$\mathbf{u}_{H,i}^T = [u_{1H,i}^{(1)}, \dots, u_{1H,i}^{(q)}] \quad (24)$$

$$\mathbf{u}_{G,i}^T = [u_{1G,i}^{(1)}, \dots, u_{1G,i}^{(r)}] \quad (25)$$

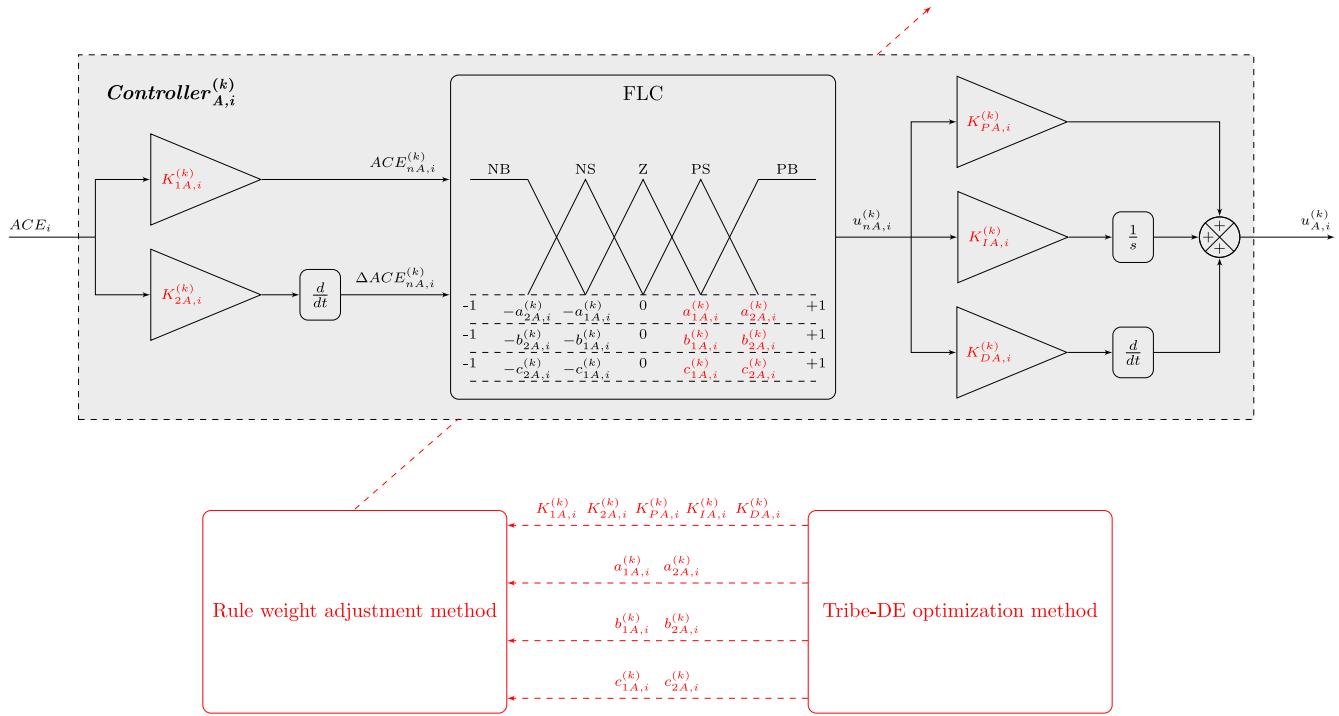


Fig. 3. The proposed controller for the k th unit (type A) in the control area i ($A = T$ for thermal unit, $A = H$ for hydro unit and $A = G$ for gas unit).

Here, the control objectives may be introduced in the following way:

Determining the control law \mathbf{u} for the system given in Eq. (17) results in desirable regulation performance in the presence of unknown disturbances \mathbf{w} and parametric uncertainties in A , B , C and D , with all states stabilized.

4. Controller design

In this paper, the fuzzy PID controller is selected to solve the LFC issue. As illustrated in Fig. 3, the fuzzy PID controller for the k th unit (type A) in the control area i was used with scaling factors $K_{1A,i}^{(k)}$ and $K_{2A,i}^{(k)}$ using $ACE_{nA,i}^{(k)}$ and $\Delta ACE_{nA,i}^{(k)}$ as the input signals. The FLC output of $u_{nA,i}^{(k)}$ is the k th normalized control input of the i th control area of the power system. The output of FLC is multiplied by the PID controller ($K_{PA,i}^{(k)}$, $K_{IA,i}^{(k)}$ and $K_{DA,i}^{(k)}$) and then summed to give the controller output of $u_{A,i}^{(k)}$. Each input/output variable membership function includes three triangular and two trapezoidal MFs with two modal parameters that are shown in Fig. 3. For instance, $a_{2A,i}^{(k)}$ is the second modal parameter of FLC first input. All the memberships of input and output are presented in five fuzzy sets of linguistic values; NB, NS, Z, PS and PB for negative big, negative small, zero, positive small and positive big, respectively. The Mamdani-type fuzzy rules are applied to express the conditional statements that comprise fuzzy logic. For defuzzifying the input/output variables, the COG method is used. All the fuzzy rules are presented in Table 2. For instance, the first fuzzy rule is as follows:

if $ACE_{nA,i}^{(k)}$ is NB and $\Delta ACE_{nA,i}^{(k)}$ is NB then $u_{nA,i}^{(k)}$ is NB with w_1 .

Where, w_1 is a rule weight that is applied to the first rule. The weight should be in the interval between zero and one, for which typically one is considered.

In this paper, the weights of fuzzy rules are dynamically adjusted using fuzzy tuning method in order to understand the importance of fuzzy rules based on the inputs at a specified time. Furthermore, the input scaling factors ($K_{1A,i}^{(k)}$ and $K_{2A,i}^{(k)}$), output

Table 2

The rule base of the fuzzy PID controller for the k th unit (type A) in the control area i .

		$\Delta ACE_{nA,i}^{(k)}$				
$ACE_{nA,i}^{(k)}$		NB	NS	Z	PS	PB
NB	NB	(w_1)	NB (w_2)	NS (w_3)	NS (w_4)	Z (w_5)
NS	NB (w_6)	NS (w_7)	NS (w_8)	Z (w_9)	PS (w_{10})	
Z	NS (w_{11})	NS (w_{12})	Z (w_{13})	PS (w_{14})	PS (w_{15})	
PS	NS (w_{16})	Z (w_{17})	PS (w_{18})	PS (w_{19})	PB (w_{20})	
PB	Z (w_{21})	PS (w_{22})	PS (w_{23})	PB (w_{24})	PB (w_{25})	

scaling factors ($K_{PA,i}^{(k)}$, $K_{IA,i}^{(k)}$ and $K_{DA,i}^{(k)}$) as well as the modal parameters of input and output MFs ($a_{1A,i}^{(k)}$, $a_{2A,i}^{(k)}$, $b_{1A,i}^{(k)}$, $b_{2A,i}^{(k)}$, $c_{1A,i}^{(k)}$ and $c_{2A,i}^{(k)}$) of each fuzzy PID controller are optimized by evolutionary algorithm, simultaneously.

4.1. The fuzzy rule weight tuning approach

Based on the number of membership functions given to the input ($ACE_{nA,i}^{(k)}$), the step response was partitioned into four main areas for the fuzzy PID controller structure as shown in Fig. 4. The required control actions based on $ACE_{nA,i}^{(k)}$ value and system response status are shown in Table 3. It should be noted that during the transient system response, the change in the value of $ACE_{nA,i}^{(k)}$ is known and therefore, the weight tuning approach can be performed through applying this error value.

Since the rule weight values must be between zero and one, the normalized error interval $[-1, 1]$ is mapped to the interval $[0, 1]$ using the following way:

$$f_1 = \left| ACE_{nA,i}^{(k)} \right| \quad (26)$$

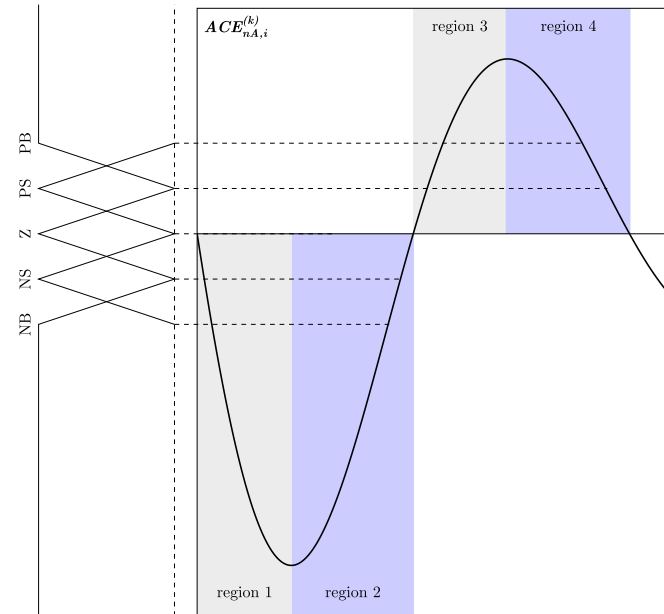
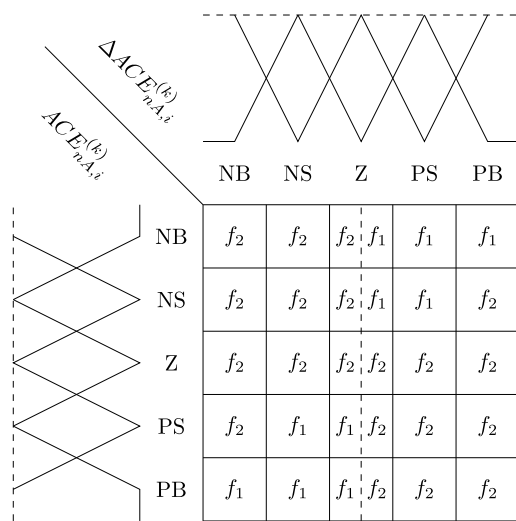
$$f_2 = 1 - \left| ACE_{nA,i}^{(k)} \right| \quad (27)$$

The self-tuning rule weights for five MFs assigned to both inputs $ACE_{nA,i}^{(k)}$ and $\Delta ACE_{nA,i}^{(k)}$ are shown in Fig. 5. According to Fig. 4, it can

Table 3

The required control action at different regions.

Region	$ACE_{nA,i}^{(k)}$	System response status	Required control action
1	Negative	Drifts apart from the zero set-point	A large negative control signal is required to prevent the undershoot
2	Negative	Approaches the zero set-point	The control signal should be reduced in time to obtain a quick response
3	Positive	Drifts apart from the zero set-point	A large positive control signal is required to prevent the overshoot
4	Positive	Approaches the zero set-point	The control signal should be increased in time to obtain a quick response

**Fig. 4.** The partitioning of the step response into regions in accordance with the ith area control error input membership functions.**Fig. 5.** The self-tuning rule weight table.

be concluded that the meta-rules for determining the rule weight of MFs at each region are done by the transient system response as given below:

- Region 1:

At this region, the fuzzy linguistic levels of $ACE_{nA,i}^{(k)}$ and $\Delta ACE_{nA,i}^{(k)}$ are $Z \rightarrow N \rightarrow NB$ and $NB \rightarrow N \rightarrow Z$, respectively.

Thus, in order to prevent undershooting, the following rule

weights should be kept at their maximum:

$$w_1 = w_2 = w_6 = w_7 = w_{11} = w_{12} = 1 - |ACE_{nA,i}^{(k)}|$$

$$w_3 = w_8 = w_{13} = 1 - |ACE_{nA,i}^{(k)}| \quad \left(\text{if } \Delta ACE_{nA,i}^{(k)} < 0 \right)$$

- Region 2:

At this region, the fuzzy linguistic levels of $ACE_{nA,i}^{(k)}$ and $\Delta ACE_{nA,i}^{(k)}$ are $NB \rightarrow N \rightarrow Z$ and $Z \rightarrow P \rightarrow PB$, respectively. Therefore, in order to achieve the required system response speed, the importance of the fuzzy rules s_1 decreases while the importance of fuzzy rules s_2 increases.

$$s_1 : w_4 = w_5 = w_9 = |ACE_{nA,i}^{(k)}|$$

$$w_3 = w_8 = |ACE_{nA,i}^{(k)}| \quad \left(\text{if } \Delta ACE_{nA,i}^{(k)} > 0 \right)$$

$$s_2 : w_{10} = w_{14} = w_{15} = 1 - |ACE_{nA,i}^{(k)}|$$

$$w_{13} = 1 - |ACE_{nA,i}^{(k)}| \quad \left(\text{if } \Delta ACE_{nA,i}^{(k)} > 0 \right)$$

- Region 3:

At this region, the fuzzy linguistic levels of $ACE_{nA,i}^{(k)}$ and $\Delta ACE_{nA,i}^{(k)}$ are $Z \rightarrow P \rightarrow PB$ and $PB \rightarrow P \rightarrow Z$, respectively. Similar to region 1, in order to prevent overshooting, the following rule weights should be kept at their maximum:

$$w_{14} = w_{15} = w_{19} = w_{20} = w_{24} = w_{25} = 1 - |ACE_{nA,i}^{(k)}|$$

$$w_{13} = w_{18} = w_{23} = 1 - |ACE_{nA,i}^{(k)}| \quad \left(\text{if } \Delta ACE_{nA,i}^{(k)} > 0 \right)$$

- Region 4:

At this region, the fuzzy linguistic levels of $ACE_{nA,i}^{(k)}$ and $\Delta ACE_{nA,i}^{(k)}$ are $PB \rightarrow P \rightarrow Z$ and $Z \rightarrow N \rightarrow NB$, respectively. According to region 2, in order to achieve the required system response speed, the weights of s_3 decreases while the weights of s_4 increases.

$$s_3 : w_{17} = w_{21} = w_{22} = |ACE_{nA,i}^{(k)}|$$

$$w_{18} = w_{23} = |ACE_{nA,i}^{(k)}| \quad \left(\text{if } \Delta ACE_{nA,i}^{(k)} < 0 \right)$$

$$s_4 : w_{11} = w_{12} = w_{16} = 1 - |ACE_{nA,i}^{(k)}|$$

$$w_{13} = 1 - |ACE_{nA,i}^{(k)}| \quad \left(\text{if } \Delta ACE_{nA,i}^{(k)} < 0 \right)$$

4.2. Optimal selection of the FLC parameters by TDE algorithm

In a well-designed LFC, by changing load in each of the areas, the proposed controller should eliminate/reduce the effect of the disturbances resulting in a safe and stable performance. In this paper, the integral of time multiplied absolute error (ITAE) corresponding to Eq. (28) is considered as the objective function

as presented below [5]:

$$J = ITAE = \int_0^{t_{sim}} \left(\sum_{i=1}^n (|\Delta F_i| + |\Delta P_{tie,i}|) \right) t \, dt \quad (28)$$

Based on this performance index J optimization problem can be stated as follows:

$$\text{minimize } J \quad (29)$$

$$\text{s. to : } 0 \leq K_{1T,i}^{(k)}, K_{2T,i}^{(k)}, K_{PT,i}^{(k)}, K_{IT,i}^{(k)}, K_{DT,i}^{(k)} \leq 2;$$

$$\text{for } i = 1, \dots, n \text{ and } k = 1, \dots, p \quad (30)$$

$$0 \leq K_{1H,i}^{(k)}, K_{2H,i}^{(k)}, K_{PH,i}^{(k)}, K_{IH,i}^{(k)}, K_{DH,i}^{(k)} \leq 2;$$

$$\text{for } i = 1, \dots, n \text{ and } k = 1, \dots, q \quad (31)$$

$$0 \leq K_{1G,i}^{(k)}, K_{2G,i}^{(k)}, K_{PG,i}^{(k)}, K_{IG,i}^{(k)}, K_{DG,i}^{(k)} \leq 2;$$

$$\text{for } i = 1, \dots, n \text{ and } k = 1, \dots, r \quad (32)$$

$$0.02 \leq a_{1T,i}^{(k)}, b_{1T,i}^{(k)}, c_{1T,i}^{(k)} < 0.35;$$

$$\text{for } i = 1, \dots, n \text{ and } k = 1, \dots, p \quad (33)$$

$$0.02 \leq a_{1H,i}^{(k)}, b_{1H,i}^{(k)}, c_{1H,i}^{(k)} < 0.35;$$

$$\text{for } i = 1, \dots, n \text{ and } k = 1, \dots, q \quad (34)$$

$$0.02 \leq a_{1G,i}^{(k)}, b_{1G,i}^{(k)}, c_{1G,i}^{(k)} < 0.35;$$

$$\text{for } i = 1, \dots, n \text{ and } k = 1, \dots, r \quad (35)$$

$$0.35 \leq a_{2T,i}^{(k)}, b_{2T,i}^{(k)}, c_{2T,i}^{(k)} \leq 0.75;$$

$$\text{for } i = 1, \dots, n \text{ and } k = 1, \dots, p \quad (36)$$

$$0.35 \leq a_{2H,i}^{(k)}, b_{2H,i}^{(k)}, c_{2H,i}^{(k)} \leq 0.75;$$

$$\text{for } i = 1, \dots, n \text{ and } k = 1, \dots, q \quad (37)$$

$$0.35 \leq a_{2G,i}^{(k)}, b_{2G,i}^{(k)}, c_{2G,i}^{(k)} \leq 0.75;$$

$$\text{for } i = 1, \dots, n \text{ and } k = 1, \dots, r \quad (38)$$

Price and Stone (1997) proposed differential evolution as a stochastic search algorithm which is a powerful method to solve optimization problems having non-linear as well as non-smooth objective functions [28].

In this paper, to overcome the defects of the original DE including speeding up the searching process and premature convergence problem, a new method called Tribe-DE (TDE) is proposed. To apply the TDE algorithm on the FLC issue, the following steps should be implemented:

- Step 1: Generation of the initial population

An initial population, including the scaling factors and the modal parameters of MFs, which must meet constraints (30)–(38), is generated randomly as follows:

$$\mathbf{ind}_{T,i}^T = [K_{1T,i}^{(1)}, K_{2T,i}^{(1)}, K_{PT,i}^{(1)}, K_{IT,i}^{(1)}, K_{DT,i}^{(1)}, a_{1T,i}^{(1)}, a_{2T,i}^{(1)}, b_{1T,i}^{(1)}, b_{2T,i}^{(1)}, c_{1T,i}^{(1)}, c_{2T,i}^{(1)}, \dots, K_{1T,i}^{(p)}, K_{2T,i}^{(p)}, K_{PT,i}^{(p)}, K_{IT,i}^{(p)}, K_{DT,i}^{(p)}, a_{1T,i}^{(p)}, a_{2T,i}^{(p)}, b_{1T,i}^{(p)}, b_{2T,i}^{(p)}, c_{1T,i}^{(p)}, c_{2T,i}^{(p)}] \quad (39)$$

$$\mathbf{ind}_{H,i}^T = [K_{1H,i}^{(1)}, K_{2H,i}^{(1)}, K_{PH,i}^{(1)}, K_{IH,i}^{(1)}, K_{DH,i}^{(1)}, a_{1H,i}^{(1)}, a_{2H,i}^{(1)}, b_{1H,i}^{(1)}, b_{2H,i}^{(1)}, c_{1H,i}^{(1)}, c_{2H,i}^{(1)}, \dots, K_{1H,i}^{(q)}, K_{2H,i}^{(q)}, K_{PH,i}^{(q)}, K_{IH,i}^{(q)}, K_{DH,i}^{(q)}, a_{1H,i}^{(q)}, a_{2H,i}^{(q)}, b_{1H,i}^{(q)}, b_{2H,i}^{(q)}, c_{1H,i}^{(q)}, c_{2H,i}^{(q)}] \quad (40)$$

$$\mathbf{ind}_{G,i}^T = [K_{1G,i}^{(1)}, K_{2G,i}^{(1)}, K_{PG,i}^{(1)}, K_{IG,i}^{(1)}, K_{DG,i}^{(1)}, a_{1G,i}^{(1)}, a_{2G,i}^{(1)}, b_{1G,i}^{(1)}, b_{2G,i}^{(1)}, c_{1G,i}^{(1)}, c_{2G,i}^{(1)}, \dots, K_{1G,i}^{(r)}, K_{2G,i}^{(r)}, K_{PG,i}^{(r)}, K_{IG,i}^{(r)}, K_{DG,i}^{(r)}, a_{1G,i}^{(r)}, a_{2G,i}^{(r)}, b_{1G,i}^{(r)}, b_{2G,i}^{(r)}, c_{1G,i}^{(r)}, c_{2G,i}^{(r)}] \quad (41)$$

$$\mathbf{ind}_m^T = [\mathbf{ind}_{T,1}^T, \mathbf{ind}_{H,1}^T, \mathbf{ind}_{G,1}^T, \dots, \mathbf{ind}_{T,n}^T, \mathbf{ind}_{H,n}^T, \mathbf{ind}_{G,n}^T] \quad (42)$$

$$\mathbf{ind}_m = \mathbf{ind}_m^{\min} + \text{rand} \times (\mathbf{ind}_m^{\max} - \mathbf{ind}_m^{\min}); \quad \text{for } m = 1, \dots, N_{ind} \quad (43)$$

- Step 2: Tribe-DE

1. Sorting the individuals:

All individuals have been sorted based on the corresponding objective function value so that the first individual has the minimum value of the objective function, as follows:

$$\mathbf{POP}_{\text{sort}} = \begin{bmatrix} \mathbf{ind}_1 \\ \mathbf{ind}_2 \\ \vdots \\ \mathbf{ind}_{N_{ind}} \end{bmatrix} \quad (44)$$

2. Partitioning the individuals into tribes:

Partitioning of individuals into tribes depends on the number of individuals in each tribe and the number of tribes. For instance, for 3 Tribes, \mathbf{ind}_1 moves to Tribe-1, \mathbf{ind}_2 moves to Tribe-2, \mathbf{ind}_3 moves to Tribe-3, \mathbf{ind}_4 moves to Tribe-1, and so on [29].

3. Linkage to tribes:

In order to find the global optimum, isolated, communing and united phases of convergence are used in the proposed algorithm, as follows:

Isolated phase: In the first phase, there is no relationship between each pair of tribes and the original DE algorithm is applied to them.

Communing phase: In this phase, the population is generated randomly from the other tribes by the mutation process.

United phase: In the third phase, all the tribes are grouped together in a group, and the original DE algorithm is used for them.

- Step 3: Mutation operation:

In this step, to cover the entire search area evenly, the mutant vectors are generated by choosing three vectors m_1 , m_2 and m_3 from initial population as $m_1 \neq m_2 \neq m_3 \neq m$. A mutant vector $\mathbf{ind}_m^{\text{mut}}$ as:

$$\mathbf{ind}_m^{\text{mut}} = \mathbf{ind}_{m_1} + \mu \times (\mathbf{ind}_{m_2} - \mathbf{ind}_{m_3}) \quad (45)$$

- Step 4: Crossover operation:

To increase the diversity, the target vector is mixed with the mutated vector, as follows:

$$\mathbf{ind}_m^{\text{new}} = \begin{cases} \mathbf{ind}_m^{\text{mut}} & \text{if } \text{rand} < c_p, \\ \mathbf{ind}_m & \text{otherwise.} \end{cases} \quad (46)$$

- Step 5: Selection criteria:

To decide on the next generation based on objective value, the following scheme is used:

$$\mathbf{ind}_m = \begin{cases} \mathbf{ind}_m^{\text{new}} & \text{if } J(\mathbf{ind}_m^{\text{new}}) < J(\mathbf{ind}_m), \\ \mathbf{ind}_m & \text{otherwise.} \end{cases} \quad (47)$$

- Step 6: Termination criteria:

Based on the predefined maximum iteration number of N_{itr} , the process is terminated.

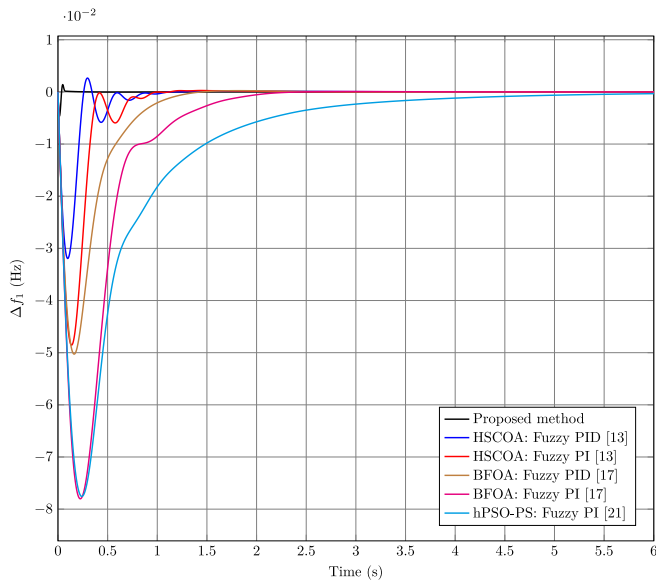


Fig. 6. Change in frequency of area 1 after 10% step load increase in area 1 for test system 1.

5. Simulation results and discussion

In this section, to demonstrate the satisfying performance of the suggested controller, three test systems are applied. In each test system, the optimal parameters of fuzzy PID controller are obtained by the proposed TDE algorithm. In addition, the objective function (ITAE) is compared with other reported optimization algorithm. The proposed algorithm's settings are as follows:

Number of tribes (N_{trb}), population (N_{ind}) and maximum iteration (N_{itr}) are 3, 24 and 50, respectively. A mutation parameter with constraint $0.2 \leq \mu \leq 0.8$ and probability of crossover $c_p = 0.2$, are considered. It should be noted that these values using the method of trial and error have been considered.

5.1. Test system 1

In this part, a two-area interconnected non-reheat thermal power system has been used to show the suggested approach effectiveness (10% SLP applied in area 1). The block diagram of the test system is available in [5], and the corresponding parameters are given in Appendix A. Table 4 lists the optimal parameters of fuzzy PID controller such as the modal parameters of MFs and the scaling factors of fuzzy PID controllers.

The comparative dynamic response for change in frequency of area 1 (Δf_1), after 10% step load increase in area 1, is shown in Fig. 6. The dynamic specifications of change in frequency of area 2 (Δf_2) and tie-line power deviations (ΔP_{tie}) of the test system 1 are also reported in Figs. 7 and 8, respectively. As shown in these figures, it is evident that the response oscillations converges smoothly to the steady value in a small time without any abrupt oscillations, thus ensuring convergence reliability of the proposed method in this paper in comparison to the other compared techniques.

Table 5 shows the comparison of the objective function (ITAE), settling time, overshoot and undershoot with different algorithms published in the literature. From the above comparisons, it can be seen that the proposed TDE in all cases except for overshooting provides a smaller value than HSCOA: Fuzzy PI/PID [13], BFOA: Fuzzy PI/PID [17] and hPSO-PS: Fuzzy PI [21]. By analysis of Table 5, the following results are found:

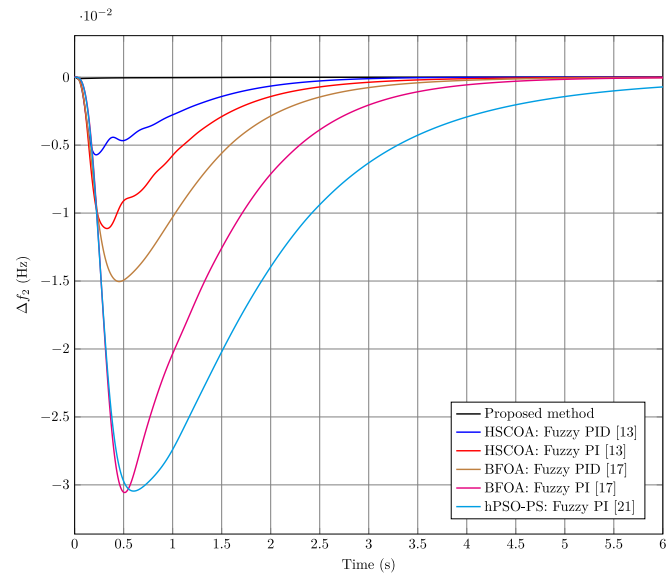


Fig. 7. Change in frequency of area 2 after 10% step load increase in area 1 for test system 1.

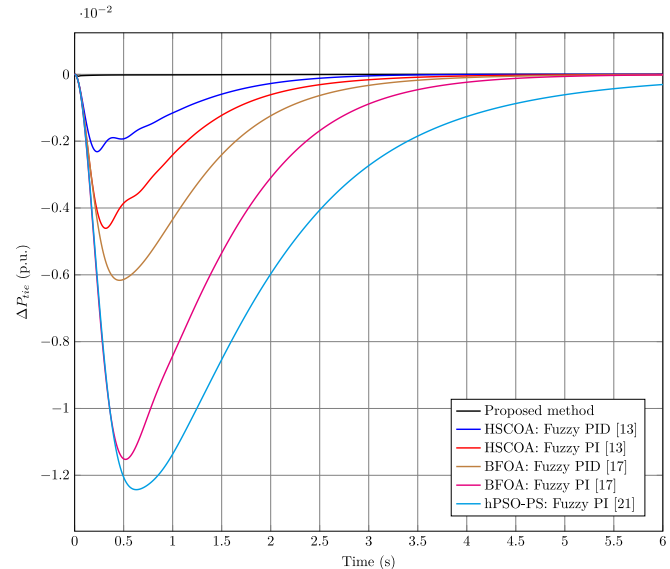


Fig. 8. Change in tie-line power after 10% step load increase in area 1 for test system 1.

- As it can be seen in this Table, it has 98.06% lower ITAE than HSCOA optimized fuzzy PID controller (ITAE = 0.0088) [13].
- Using the proposed method in this paper causes 92.57% less settling time and 47.60% decrease in maximum overshoot than those reported in [13], for the regulation of variable Δf_1 .
- Compared to the method proposed in [13], the use of the controller suggested in this paper for the regulation of Δf_1 , Δf_2 and ΔP_{tie} , shows 85.52%, 97.70% and 97.56% decrease in the absolute maximum undershoot, respectively.

5.1.1. Sensitivity analysis of test system 1

In order to identify the robustness of a close-loop system, evaluating the dynamic behavior of power system is inevitable by taking into account the wide variations of loading condition and system parameters. For the validity of the proposed method,

Table 4

Optimal values of controller parameters for test system 1.

Area 1	$K_{1T,1}^{(1)}$ 1.8321	$K_{2T,1}^{(1)}$ 0.1858	$K_{PT,1}^{(1)}$ 1.9921	$K_{IT,1}^{(1)}$ 1.8558	$K_{DT,1}^{(1)}$ 0.4115	$a_{1T,1}^{(1)}$ 0.02	$a_{2T,1}^{(1)}$ 0.4035	$b_{1T,1}^{(1)}$ 0.34	$b_{2T,1}^{(1)}$ 0.5018	$c_{1T,1}^{(1)}$ 0.02	$c_{2T,1}^{(1)}$ 0.75
Area 2	$K_{1T,2}^{(1)}$ 1.5546	$K_{2T,2}^{(1)}$ 1.8747	$K_{PT,2}^{(1)}$ 1.2981	$K_{IT,2}^{(1)}$ 0.8192	$K_{DT,2}^{(1)}$ 0.2734	$a_{1T,2}^{(1)}$ 0.0215	$a_{2T,2}^{(1)}$ 0.75	$b_{1T,2}^{(1)}$ 0.1686	$b_{2T,2}^{(1)}$ 0.7035	$c_{1T,2}^{(1)}$ 0.2992	$c_{2T,2}^{(1)}$ 0.7104

Table 5

Comparative analysis of various tuning method based fuzzy PI/PID controller for test system 1.

Controller	ITAE	Settling time (s)			Overshoot			Undershoot (-ve)		
		Δf_1	Δf_2	ΔP_{tie}	Δf_1 (Hz)	Δf_2 (Hz)	ΔP_{tie} (p.u.)	Δf_1 (Hz)	Δf_2 (Hz)	ΔP_{tie} (p.u.)
Proposed method	1.71e-04	0.061	0	0	0.0014	0	0	0.0046	1.31e-04	5.64e-05
HSCOA: Fuzzy PID [13]	0.0088	0.821	2.161	1.616	0.0027	0	1.45e-07	0.0319	0.0057	0.0023
HSCOA: Fuzzy PI [13]	0.0192	0.922	2.774	2.144	2.73e-04	0	0	0.0485	0.0111	0.0046
BFOA: Fuzzy PID [17]	0.0364	1.262	3.343	2.679	2.38e-04	0	0	0.0503	0.0150	0.0062
BFOA: Fuzzy PI [17]	0.0825	2.019	4.096	3.436	7.76e-05	0	0	0.0780	0.0306	0.0115
hPSO-PS: Fuzzy PI [21]	0.2044	5.369	6.540	5.282	0	0	0	0.0776	0.0305	0.0124

Table 6

Sensitivity analysis of test system 1.

Controller	Parameters	% of change	ITAE	Settling time (s)			Undershoot (-ve)		
				Δf_1	Δf_2	ΔP_{tie}	Δf_1 (Hz)	Δf_2 (Hz)	ΔP_{tie} (p.u.)
Proposed method	$T_{GT,1}^{(1)}$ and $T_{GT,2}^{(1)}$	+50	1.89e-04	0.091	0	0	0.0067	2.70e-04	1.16e-04
		+25	1.82e-04	0.076	0	0	0.0057	1.93e-04	8.34e-05
	$T_{IT,1}^{(1)}$ and $T_{IT,2}^{(1)}$	+50	1.86e-04	0.086	0	0	0.0068	2.88e-04	1.25e-04
		-50	1.97e-04	0.038	0	0	0.0025	3.76e-05	1.58e-05
	T_{12}	-25	1.90e-04	0.060	0	0	0.0046	9.90e-05	4.25e-05
		-50	2.43e-04	0.059	0	0	0.0046	6.64e-05	2.85e-05
	B_1 and B_2	-25	1.90e-04	0.065	0	0	0.0048	1.81e-04	5.93e-05
		-50	2.61e-04	0.072	0	0	0.0052	2.96e-04	6.81e-05
	$R_{T,1}^{(1)}$ and $R_{T,2}^{(1)}$	-25	1.72e-04	0.061	0	0	0.0046	1.31e-04	5.64e-05
		-50	1.72e-04	0.061	0	0	0.0046	1.31e-04	5.64e-05
HSCOA: Fuzzy PID [13]	$T_{GT,1}^{(1)}$ and $T_{GT,2}^{(1)}$	+50	0.0108	1.376	2.172	1.602	0.0397	0.0086	0.0033
		+25	0.0095	0.970	2.157	1.603	0.0360	0.0071	0.0028
	$T_{IT,1}^{(1)}$ and $T_{IT,2}^{(1)}$	+50	0.0108	1.476	1.997	1.536	0.0424	0.0099	0.0040
		-50	0.0096	1.224	2.337	1.751	0.0205	0.0032	0.0014
	T_{12}	-25	0.0107	0.827	2.370	1.764	0.0321	0.0044	0.0018
		-50	0.0147	2.514	2.760	1.983	0.0323	0.0032	0.0014
	B_1 and B_2	-25	0.0100	1.157	2.169	1.496	0.0362	0.0093	0.0028
		-50	0.0156	1.603	2.291	1.362	0.0430	0.0179	0.0035
	$R_{T,1}^{(1)}$ and $R_{T,2}^{(1)}$	-25	0.0091	0.821	2.174	1.633	0.0319	0.0057	0.0023
		-50	0.0100	0.985	2.200	1.667	0.0318	0.0056	0.0023

changing the operating load conditions and some important system parameters have been studied such as $T_{GT,1}^{(1)}$, $T_{GT,2}^{(1)}$, $T_{IT,1}^{(1)}$, $T_{IT,2}^{(1)}$, T_{12} , B_1 , B_2 , $R_{T,1}^{(1)}$ and $R_{T,2}^{(1)}$ in the range of $\pm 25\%$ and $\pm 50\%$ of the nominal values, and some of the worst cases are compared with the method presented in reference [13] (Table 6). As seen in this Table, the proposed fuzzy PID controller in all cases provides better solutions than the solutions of HSCOA optimized fuzzy PID controller [13], in terms of ITAE, settling time and absolute maximum undershoot.

Also, the tie-line and frequency deviations of the power system under two worst cases are shown in Figs. 9–11. As shown in these figures, the proposed controller is more robust to the method presented in [13] in the face of parametric uncertainties -50% in T_{12} and -50% in B_1 and B_2 .

5.2. Test system 2

In this section, LFC issue in a two area interconnected multi-source power system is presented in order to emphasize the capability of the proposed fuzzy PID controller method. Each area of the power system is equipped with various generations including a reheat thermal unit, a hydro unit and a gas unit. In this test system, the following two scenarios are studied:

- Scenario 1: Two-area interconnected multi-source power system with AC tie-lines.
- Scenario 2: Two-area interconnected multi-source power system with AC-DC parallel tie-lines.

A 1% SLP is applied in area 1 to study the dynamic behavior of both of the power systems (with and without HVDC link). The parameters applied in this test system in both scenarios are shown in Appendix B. Detailed information about this power system are also given in [30].

5.2.1. Scenario 1

The modal parameters of MFs and the scaling factors of fuzzy PID controllers adjusted by TDE are listed in Table 7. The comparative dynamic response for change in frequency of area 1 and 2 (Δf_1 and Δf_2) and tie-line power (ΔP_{tie}) after 1% step load increase in area 1, are shown in Figs. 12–14, respectively. These figures demonstrate that the method suggested here shows the acceptable steady state and transient response characteristics.

Also, the comparative results for test system 2 with just AC tie-line for proposed controller and HSCOA optimized fuzzy PID controller [13] are tabulated in Table 8. By comparing the results, the following conclusions can be drawn:

Table 7

Optimal values of controller parameters for test system 2 with just AC tie-line.

Area 1	Thermal	$K_{1T,1}^{(1)}$ 1.8078	$K_{2T,1}^{(1)}$ 0.2169	$K_{PT,1}^{(1)}$ 1.9116	$K_{IT,1}^{(1)}$ 0.1621	$K_{DT,1}^{(1)}$ 0.2883	$a_{1T,1}^{(1)}$ 0.0500	$a_{2T,1}^{(1)}$ 0.4075	$b_{1T,1}^{(1)}$ 0.0624	$b_{2T,1}^{(1)}$ 0.4009	$c_{1T,1}^{(1)}$ 0.0500	$c_{2T,1}^{(1)}$ 0.4451
	Hydro	$K_{1H,1}^{(1)}$ 0.3000	$K_{2H,1}^{(1)}$ 0.0972	$K_{PH,1}^{(1)}$ 1.3337	$K_{IH,1}^{(1)}$ 0.4326	$K_{DH,1}^{(1)}$ 0.4761	$a_{1H,1}^{(1)}$ 0.0500	$a_{2H,1}^{(1)}$ 0.3759	$b_{1H,1}^{(1)}$ 0.1373	$b_{2H,1}^{(1)}$ 0.3578	$c_{1H,1}^{(1)}$ 0.1392	$c_{2H,1}^{(1)}$ 0.3636
	Gas	$K_{1G,1}^{(1)}$ 1.9019	$K_{2G,1}^{(1)}$ 0.0271	$K_{PG,1}^{(1)}$ 1.3077	$K_{IG,1}^{(1)}$ 1.9035	$K_{DG,1}^{(1)}$ 0.1945	$a_{1G,1}^{(1)}$ 0.0500	$a_{2G,1}^{(1)}$ 0.4500	$b_{1G,1}^{(1)}$ 0.1435	$b_{2G,1}^{(1)}$ 0.4338	$c_{1G,1}^{(1)}$ 0.0500	$c_{2G,1}^{(1)}$ 0.4500
Area 2	Thermal	$K_{1T,2}^{(1)}$ 1.8141	$K_{2T,2}^{(1)}$ 0.2333	$K_{PT,2}^{(1)}$ 1.8580	$K_{IT,2}^{(1)}$ 0.1561	$K_{DT,2}^{(1)}$ 0.1302	$a_{1T,2}^{(1)}$ 0.1500	$a_{2T,2}^{(1)}$ 0.4291	$b_{1T,2}^{(1)}$ 0.0586	$b_{2T,2}^{(1)}$ 0.3520	$c_{1T,2}^{(1)}$ 0.0708	$c_{2T,2}^{(1)}$ 0.3899
	Hydro	$K_{1H,2}^{(1)}$ 0.3847	$K_{2H,2}^{(1)}$ 0.1142	$K_{PH,2}^{(1)}$ 1.3457	$K_{IH,2}^{(1)}$ 0.4959	$K_{DH,2}^{(1)}$ 0.3975	$a_{1H,2}^{(1)}$ 0.1027	$a_{2H,2}^{(1)}$ 0.3953	$b_{1H,2}^{(1)}$ 0.0988	$b_{2H,2}^{(1)}$ 0.3774	$c_{1H,2}^{(1)}$ 0.1120	$c_{2H,2}^{(1)}$ 0.3551
	Gas	$K_{1G,2}^{(1)}$ 1.8995	$K_{2G,2}^{(1)}$ 0.0414	$K_{PG,2}^{(1)}$ 1.4133	$K_{IG,2}^{(1)}$ 1.9138	$K_{DG,2}^{(1)}$ 0.1317	$a_{1G,2}^{(1)}$ 0.1199	$a_{2G,2}^{(1)}$ 0.3674	$b_{1G,2}^{(1)}$ 0.0824	$b_{2G,2}^{(1)}$ 0.3532	$c_{1G,2}^{(1)}$ 0.1460	$c_{2G,2}^{(1)}$ 0.3500

Table 8

Comparative analysis for test system 2 with just AC tie-line.

Controller	ITAE	Settling time (s)			Overshoot			Undershoot (-ve)		
		Δf_1	Δf_2	ΔP_{tie}	Δf_1 (Hz)	Δf_2 (Hz)	ΔP_{tie} (p.u.)	Δf_1 (Hz)	Δf_2 (Hz)	ΔP_{tie} (p.u.)
Proposed method	0.0019	0.293	0	0	2.40e-05	5.37e-06	0	0.0022	3.03e-04	1.05e-04
HSCOA: Fuzzy PID [13]	0.0085	0.725	2.177	0.861	8.78e-05	9.82e-05	3.85e-08	0.0074	0.0018	5.85e-04

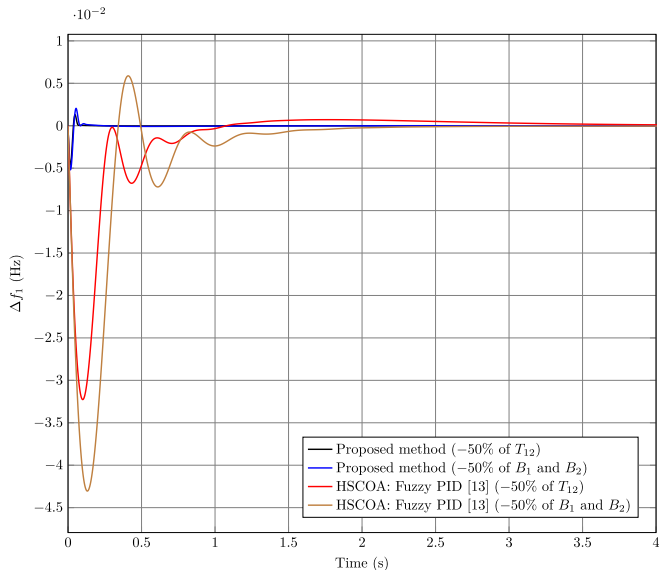


Fig. 9. Sensitivity analysis of test system 1 (frequency deviation of area 1).

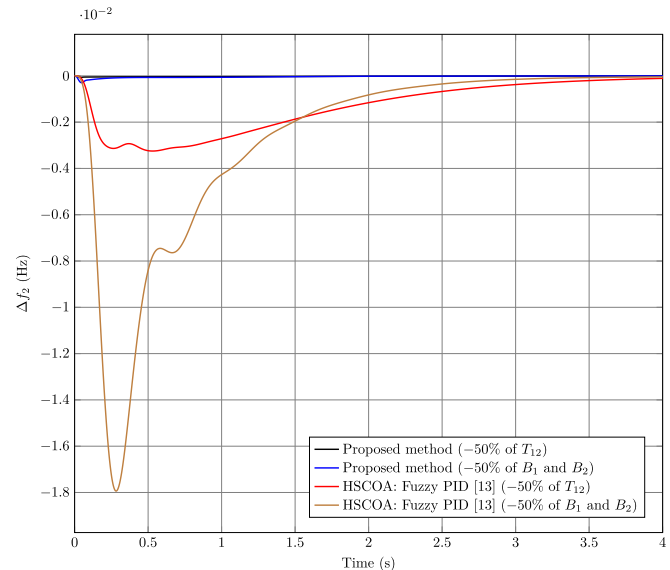


Fig. 10. Sensitivity analysis of test system 1 (frequency deviation of area 2).

- Compared to the proposed method in reference [13], the use of the controller suggested in this paper shows 77.65 percent decrease in ITAE.
- Applying the method presented in the present paper rather than the controller suggested in reference [13] brings about 70.27, 83.17 and 82.12 percent less absolute maximum undershoot for the regulation of Δf_1 , Δf_2 and ΔP_{tie} , respectively.
- Through using the method suggested in this article, the variable Δf_1 is regulated with a settling time of 0.293 s, a peak overshoot of 2.40e-05 Hz and a maximum absolute undershoot of 0.0022 Hz, however, using the method presented in reference [13], this variable will be regulated with a settling time of 0.725 s, a maximum overshoot of 8.78e-05 Hz and a maximum absolute undershoot of 0.0074 Hz.

Similar to Section 5.1.1, sensitivity analysis of the test system 2 with AC tie-lines has been studied and the worst case (parametric

uncertainty +50% in B_1 and B_2) is compared with the method presented in reference [13]. The comparison results are shown in Figs. 15–17 and Table 9. As shown in these figures, it is clearly seen that the use of the controller suggested by reference [13] has not been able to eliminate the tie-line and frequency deviations. However, the response deviations converge smoothly to the steady value in a small time through using the controller proposed in this paper. Thus, using the on-line fuzzy rule weight adjustment method ensure convergence reliability and robustness of this controller against with parametric uncertainties.

Furthermore, another simulation has been performed in this scenario through increasing the uncertainty considered in the previous simulation to investigate the effect of using or not using the proposed on-line rule weight tuning method on the overall system response. The two states are compared after +200% uncertainty in parameters B_1 and B_2 in Figs. 18–20. As can be seen in these figures, the system's steady state response will not converge

Table 9

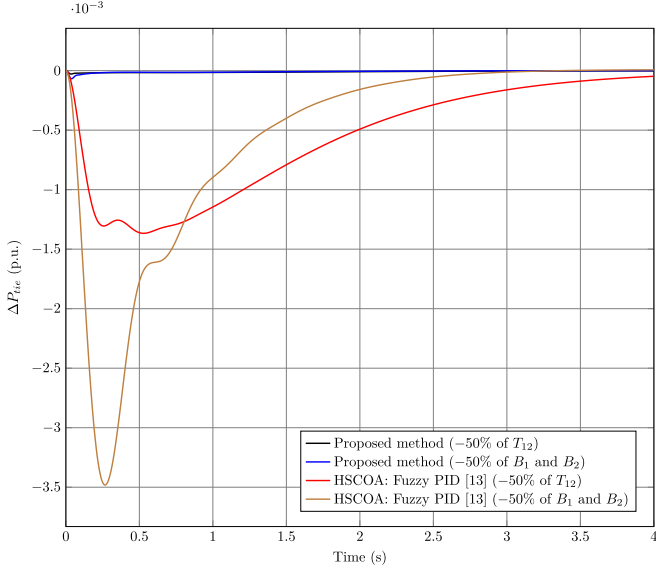
Sensitivity analysis of test system 2 with just AC tie-line.

Controller	ITAE	Settling time (s)			Overshoot			Undershoot ($-ve$)		
		Δf_1	Δf_2	ΔP_{tie}	Δf_1 (Hz)	Δf_2 (Hz)	ΔP_{tie} (p.u.)	Δf_1 (Hz)	Δf_2 (Hz)	ΔP_{tie} (p.u.)
Proposed method	0.0018	0.227	0	0	2.58e-05	6.04e-06	0	0.0019	1.57e-04	7.79e-05
HSCOA: Fuzzy PID [13]	0.1929	NaN	NaN	0	0.0016	0.0016	8.86e-05	0.0070	0.0019	4.76e-04

Table 10

Optimal values of controller parameters for test system 2 with HVDC link.

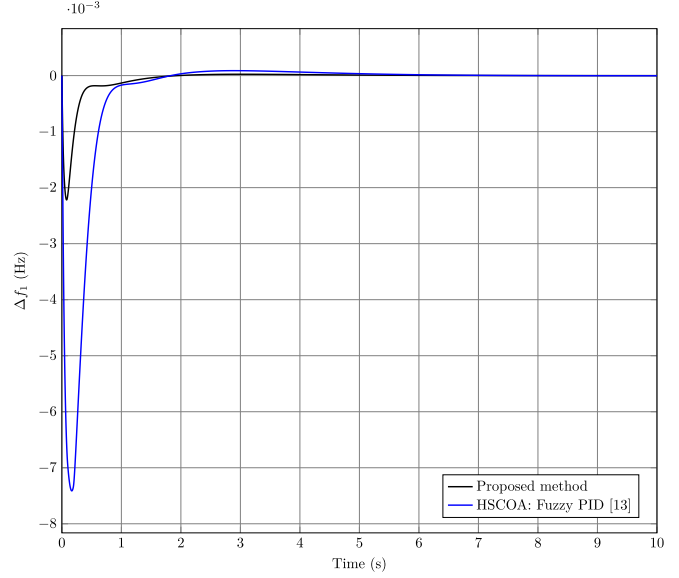
Area 1	Thermal	$K_{1T,1}^{(1)}$ 1.4142	$K_{2T,1}^{(1)}$ 1.9349	$K_{PT,1}^{(1)}$ 1.0284	$K_{1T,1}^{(1)}$ 1.9355	$K_{DT,1}^{(1)}$ 0.2526	$a_{1T,1}^{(1)}$ 0.0200	$a_{2T,1}^{(1)}$ 0.6483	$b_{1T,1}^{(1)}$ 0.2736	$b_{2T,1}^{(1)}$ 0.4571	$c_{1T,1}^{(1)}$ 0.0200	$c_{2T,1}^{(1)}$ 0.6144
	Hydro	$K_{1H,1}^{(1)}$ 1.8409	$K_{2H,1}^{(1)}$ 0.1465	$K_{PH,1}^{(1)}$ 2.0000	$K_{1H,1}^{(1)}$ 0.0010	$K_{DH,1}^{(1)}$ 0.1525	$a_{1H,1}^{(1)}$ 0.3400	$a_{2H,1}^{(1)}$ 0.5710	$b_{1H,1}^{(1)}$ 0.0200	$b_{2H,1}^{(1)}$ 0.5184	$c_{1H,1}^{(1)}$ 0.3400	$c_{2H,1}^{(1)}$ 0.4458
	Gas	$K_{1G,1}^{(1)}$ 1.7876	$K_{2G,1}^{(1)}$ 0.2344	$K_{PG,1}^{(1)}$ 1.7452	$K_{1G,1}^{(1)}$ 1.7505	$K_{DG,1}^{(1)}$ 0.2345	$a_{1G,1}^{(1)}$ 0.0200	$a_{2G,1}^{(1)}$ 0.5490	$b_{1G,1}^{(1)}$ 0.0200	$b_{2G,1}^{(1)}$ 0.4756	$c_{1G,1}^{(1)}$ 0.0800	$c_{2G,1}^{(1)}$ 0.6114
Area 2	Thermal	$K_{1T,2}^{(1)}$ 1.1814	$K_{2T,2}^{(1)}$ 1.9975	$K_{PT,2}^{(1)}$ 0.9816	$K_{1T,2}^{(1)}$ 1.9765	$K_{DT,2}^{(1)}$ 0.2526	$a_{1T,2}^{(1)}$ 0.0200	$a_{2T,2}^{(1)}$ 0.5293	$b_{1T,2}^{(1)}$ 0.0614	$b_{2T,2}^{(1)}$ 0.4434	$c_{1T,2}^{(1)}$ 0.0888	$c_{2T,2}^{(1)}$ 0.5368
	Hydro	$K_{1H,2}^{(1)}$ 1.8639	$K_{2H,2}^{(1)}$ 0.0506	$K_{PH,2}^{(1)}$ 1.8551	$K_{1H,2}^{(1)}$ 0.2016	$K_{DH,2}^{(1)}$ 0.0100	$a_{1H,2}^{(1)}$ 0.0200	$a_{2H,2}^{(1)}$ 0.5592	$b_{1H,2}^{(1)}$ 0.0888	$b_{2H,2}^{(1)}$ 0.5283	$c_{1H,2}^{(1)}$ 0.1706	$c_{2H,2}^{(1)}$ 0.4800
	Gas	$K_{1G,2}^{(1)}$ 1.9091	$K_{2G,2}^{(1)}$ 0.0244	$K_{PG,2}^{(1)}$ 1.5696	$K_{1G,2}^{(1)}$ 1.9337	$K_{DG,2}^{(1)}$ 0.2486	$a_{1G,2}^{(1)}$ 0.0269	$a_{2G,2}^{(1)}$ 0.5037	$b_{1G,2}^{(1)}$ 0.3191	$b_{2G,2}^{(1)}$ 0.5898	$c_{1G,2}^{(1)}$ 0.0200	$c_{2G,2}^{(1)}$ 0.6500

**Fig. 11.** Sensitivity analysis of test system 1 (change of tie-line power).

to zero if the on-line rule weight tuning method is not applied. While using the proposed on-line tuning method, the frequency and tie-line deviations converges to zero even with uncertainty much higher than +200%. As an example, the convergence of weight parameters w_1 and w_4 belonging to the controller of area 1 is shown in Fig. 21. The adaptation process of these two parameters is based on Eqs. (26) and (27), respectively. Therefore, it can be concluded that the use of the on-line error-based rule weight tuning method for fuzzy PID controllers reduces the sensitivity to parametric uncertainties.

5.2.2. Scenario 2

Similarly, the optimal values of controller parameters for test system 2 with HVDC link are listed in Table 10. The dynamic responses of change in frequency of area 1 and 2 (Δf_1 and Δf_2) and tie-line power (ΔP_{tie}) for the test system 2 with HVDC link are illustrated in Figs. 22–24 for 1%–3% SLP applied in area 1. As shown in these figures, it is evident that the performance of

**Fig. 12.** Change in frequency of area 1 after 1% step load increase in area 1 for test system 2 with just AC tie-line.

proposed fuzzy PID controller in comparison with [13] provides proper dynamic responses and robustness against the step load perturbation.

Furthermore, the comparative results obtained from the proposed method and HSCOA optimized fuzzy PID controller [13] in terms of ITAE, settling time and undershoot are tabulated in Table 11, in different SLPs. From the above Table, it is evident that the adjusted gains of the specific controller structure give excellent results showing that the proposed algorithm is so robust.

Additionally, the robustness of the controller proposed in this paper and the controller suggested by reference [13] for the test system 2 with HVDC link is studied under a random step load pattern shown in Fig. 25 [13]. The comparative dynamic response for change in frequency of areas 1 and 2 and tie-line power after random step load change in area 1, are shown in Figs. 26–28, respectively. These figures demonstrate that the

Table 11

Comparative analysis in different SLP in area 1 for test system 2 with HVDC link.

Controller	SLP (%)	ITAE	Settling time (s)			Undershoot ($-ve$)		
			Δf_1	Δf_2	ΔP_{tie}	Δf_1 (Hz)	Δf_2 (Hz)	ΔP_{tie} (p.u.)
Proposed method	1	4.03e-04	0.089	0	0	8.67e-04	7.00e-05	3.01e-05
	2	0.0041	1.389	1.2720	0.635	0.0097	0.0014	5.84e-04
	3	0.0108	2.113	2.055	1.403	0.0210	0.0034	0.0014
HSCOA: Fuzzy PID [13]	1	0.0093	0.714	2.671	1.215	0.0076	0.0015	6.83e-05
	2	0.0216	1.076	3.800	2.476	0.0179	0.0036	0.0017
	3	0.0347	1.151	4.213	2.951	0.0267	0.0054	0.0025

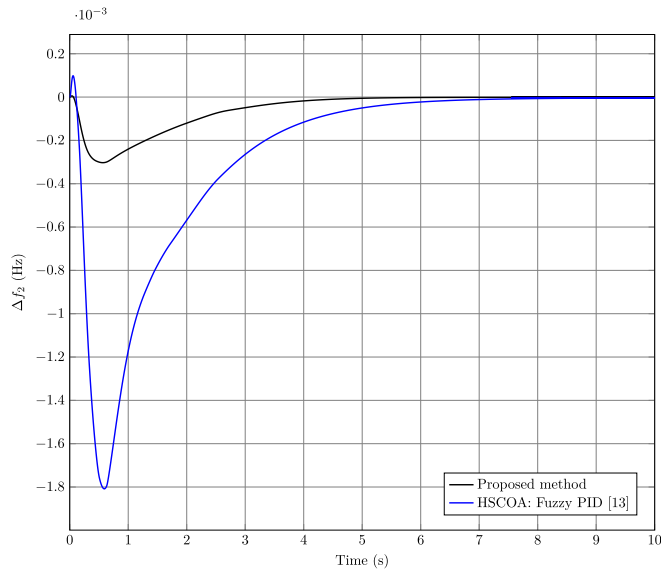


Fig. 13. Change in frequency of area 2 after 1% step load increase in area 1 for test system 2 with just AC tie-line.

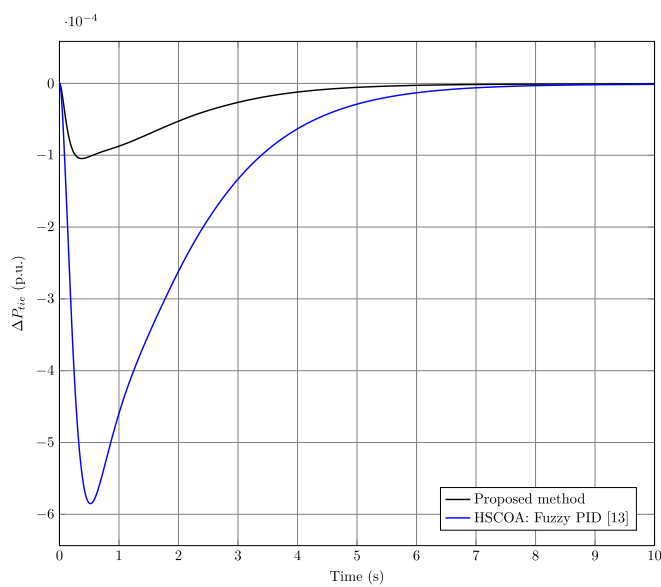


Fig. 14. Change in tie-line power after 1% step load increase in area 1 for test system 2 with just AC tie-line.

method suggested here achieved superior damping of the tie-line and frequency deviations than the method suggested by

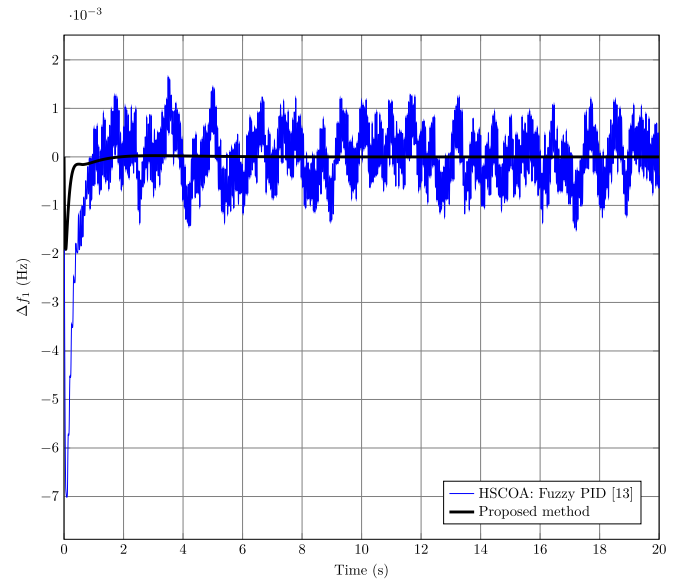


Fig. 15. Sensitivity analysis of test system 2 with just AC tie-line (frequency deviation of area 1).

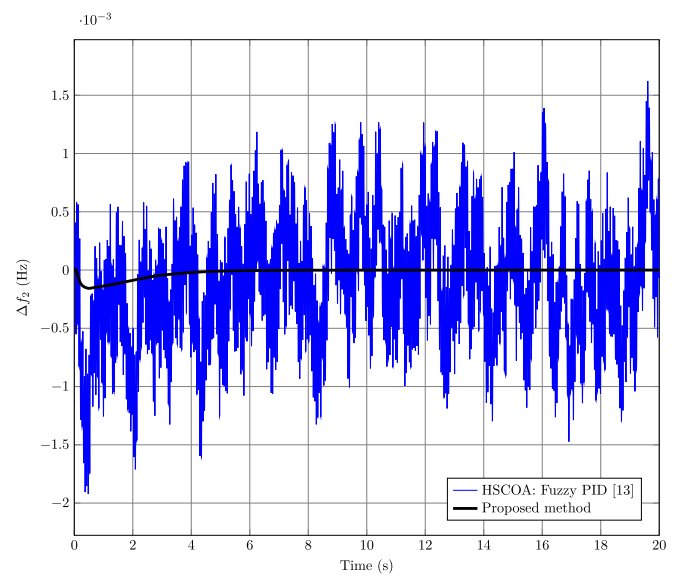


Fig. 16. Sensitivity analysis of test system 2 with just AC tie-line (frequency deviation of area 2).

reference [13] which shows the acceptable transient and steady state response characteristics.

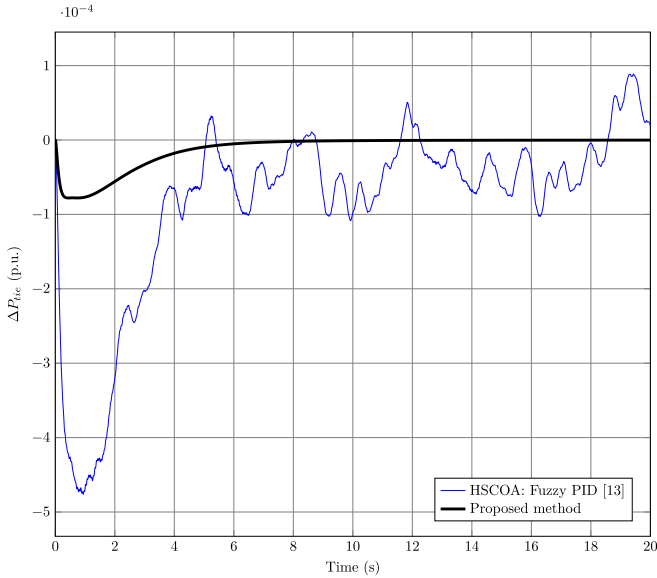


Fig. 17. Sensitivity analysis of test system 2 with just AC tie-line (change of tie-line power).

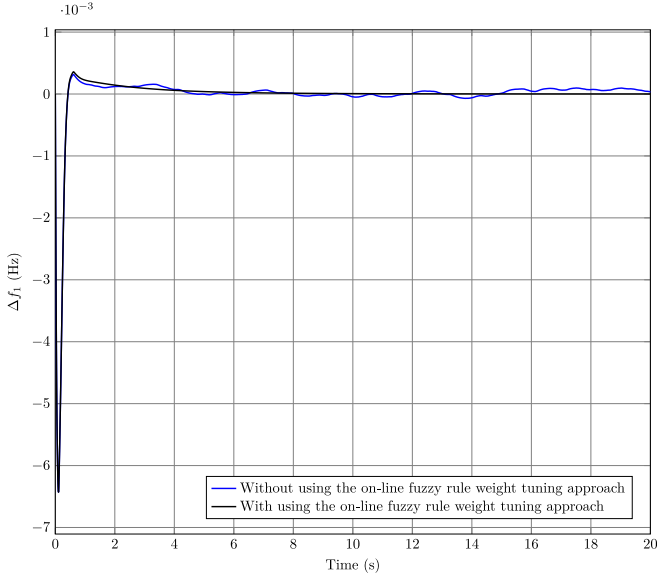


Fig. 18. Frequency deviation of area 1 for test system 2 with just AC tie-line (Parametric uncertainty +200% in B_1 and B_2).

5.3. Test system 3

Finally, to demonstrate the capability of the suggested method to deal with nonlinearity, the study is extended to a three area nonlinear system [31–33]. In each of these three areas, there is a single reheat turbine with a generation rate constraint (GRC) of 3% per minute. The block diagram of this system is available in [31], while the nominal system parameters are given in Appendix C. The modal parameters of MFs and the scaling factors of fuzzy PID controllers tuned by TDE are shown in Table 12. The dynamic response for Δf_1 , Δf_2 , Δf_3 , $\Delta P_{tie,12}$, $\Delta P_{tie,13}$ and $\Delta P_{tie,23}$ after 1% step load perturbation in area 1, are shown in Figs. 29–34, respectively. Furthermore, the settling time and the objective function (ITAE) of the responses obtained by different methods are noted in Table 13. As seen in this Table, the proposed controller provides better responses than the responses of PID,

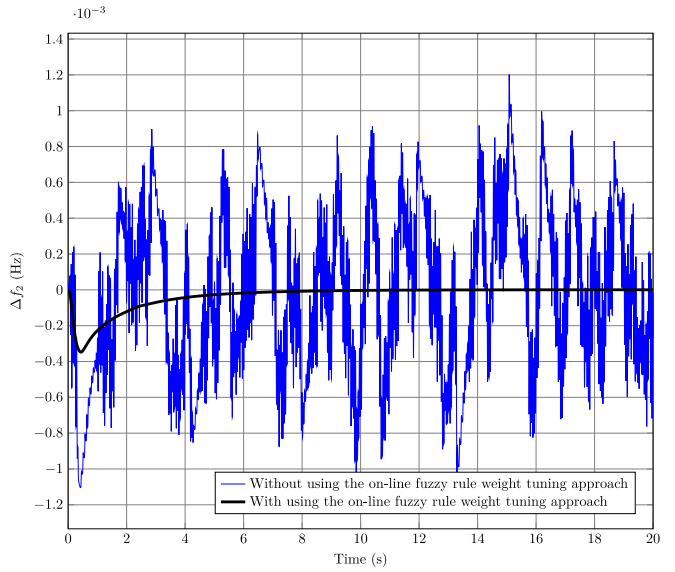


Fig. 19. Frequency deviation of area 2 for test system 2 with just AC tie-line (Parametric uncertainty +200% in B_1 and B_2).

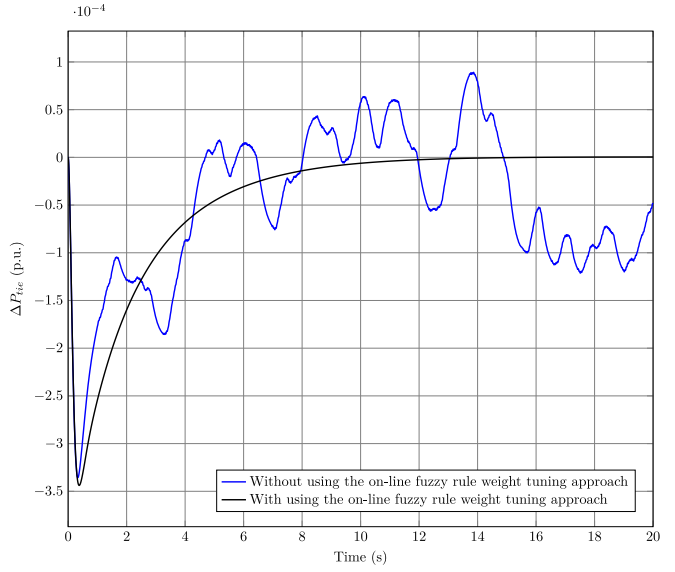


Fig. 20. Change of tie-line power for test system 2 with just AC tie-line (Parametric uncertainty +200% in B_1 and B_2).

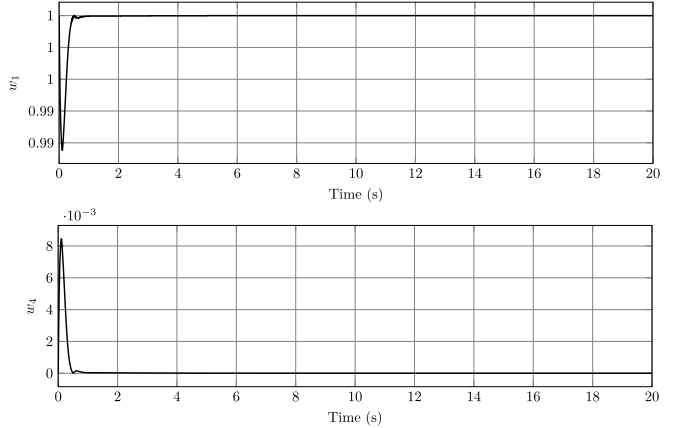
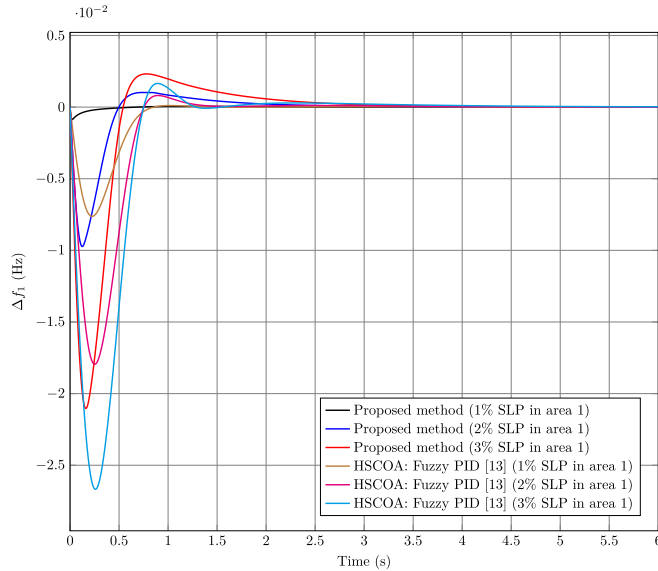
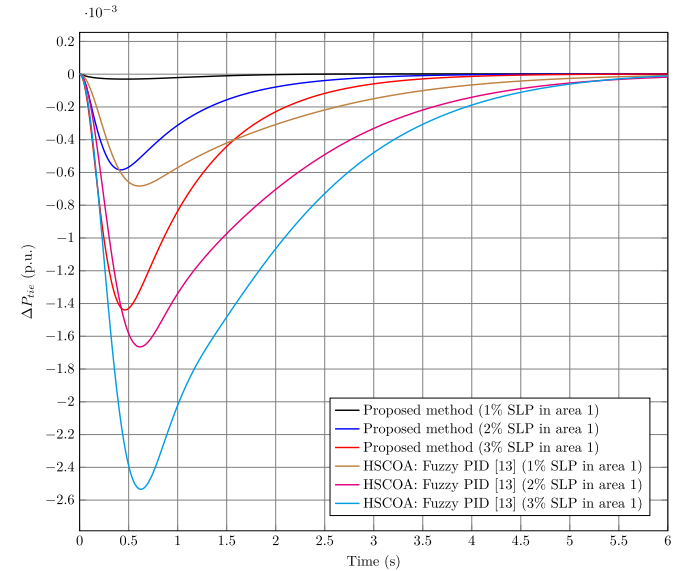
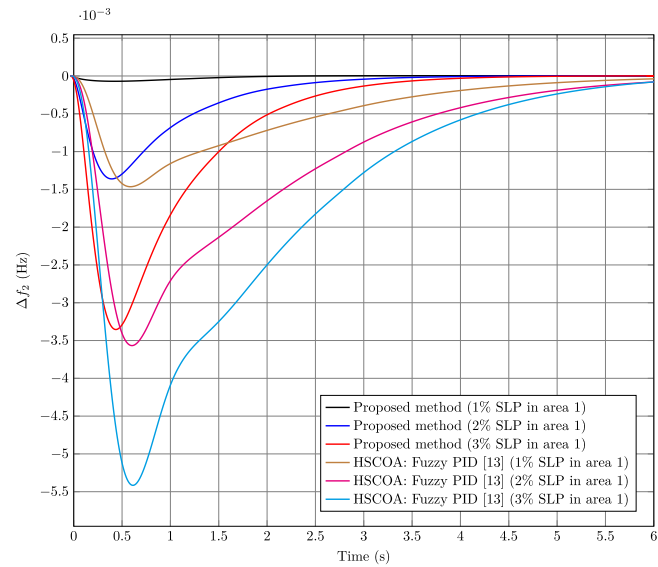
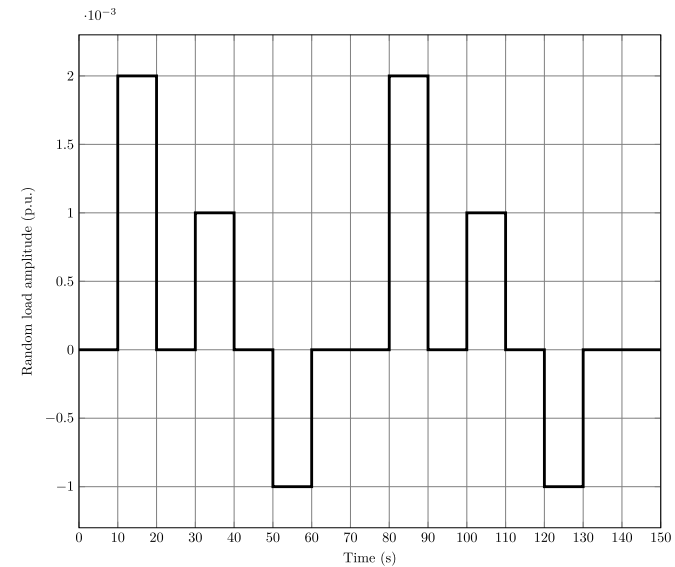


Fig. 21. The convergence of weight parameters w_1 and w_4 belong to the controller of area 1 in test system 2 with just AC tie-line.

Table 12

Optimal values of controller parameters for test system 3.

Area 1	$K_{1T,1}^{(1)}$ 1.1957	$K_{2T,1}^{(1)}$ 0.3542	$K_{PT,1}^{(1)}$ 0.5955	$K_{IT,1}^{(1)}$ 1.7858	$K_{DT,1}^{(1)}$ 0.5682	$a_{1T,1}^{(1)}$ 0.0384	$a_{2T,1}^{(1)}$ 0.5491	$b_{1T,1}^{(1)}$ 0.0658	$b_{2T,1}^{(1)}$ 0.4930	$c_{1T,1}^{(1)}$ 0.0658	$c_{2T,1}^{(1)}$ 0.4024
Area 2	$K_{1T,2}^{(1)}$ 0.5100	$K_{2T,2}^{(1)}$ 1.4291	$K_{PT,2}^{(1)}$ 0.7704	$K_{IT,2}^{(1)}$ 2	$K_{DT,2}^{(1)}$ 0.2526	$a_{1T,2}^{(1)}$ 0.0817	$a_{2T,2}^{(1)}$ 0.5542	$b_{1T,2}^{(1)}$ 0.0858	$b_{2T,2}^{(1)}$ 0.35	$c_{1T,2}^{(1)}$ 0.2590	$c_{2T,2}^{(1)}$ 0.5681
Area 3	$K_{1T,3}^{(1)}$ 1.1247	$K_{2T,3}^{(1)}$ 1.1106	$K_{PT,3}^{(1)}$ 0.3772	$K_{IT,3}^{(1)}$ 2	$K_{DT,3}^{(1)}$ 0.2906	$a_{1T,3}^{(1)}$ 0.1495	$a_{2T,3}^{(1)}$ 0.65	$b_{1T,3}^{(1)}$ 0.2250	$b_{2T,3}^{(1)}$ 0.65	$c_{1T,3}^{(1)}$ 0.2993	$c_{2T,3}^{(1)}$ 0.3829

**Fig. 22.** Change in frequency of area 1 in different SLP in area 1 for test system 2 with HVDC link.**Fig. 24.** Change in tie-line power in different SLP in area 1 for test system 2 with HVDC link.**Fig. 23.** Change in frequency of area 2 in different SLP in area 1 for test system 2 with HVDC link.**Fig. 25.** Random load pattern.

2DOF IDD and cascade PD-PID controllers [31–33], in term of settling time. It should be noted that the numbers in parentheses in Table 13 indicate the percentage of settling time improved by the method proposed in this paper compared to the other methods.

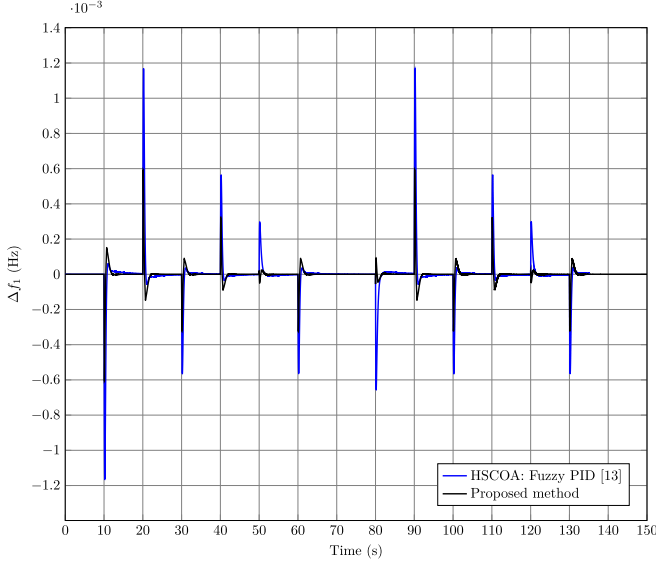
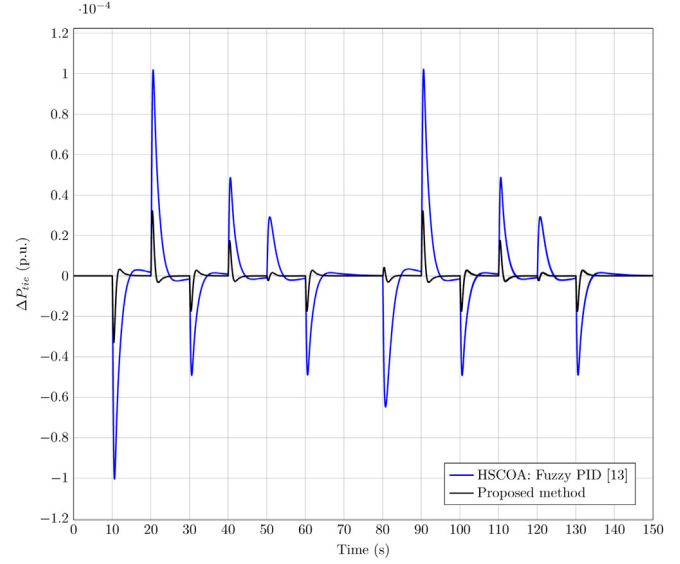
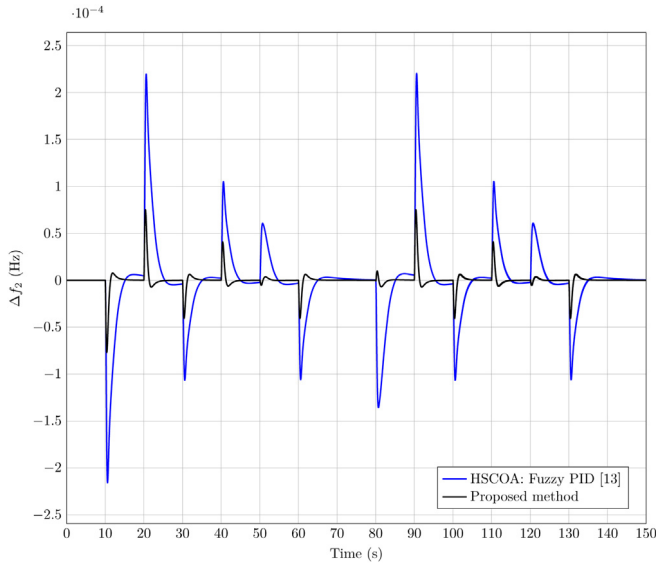
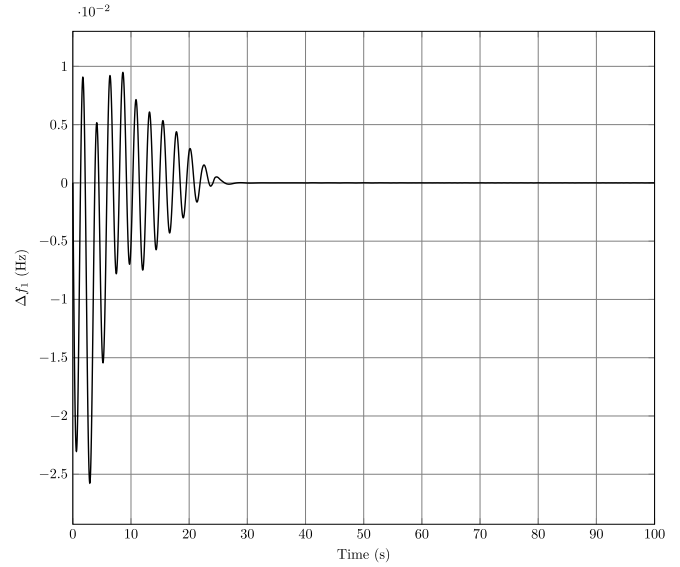
6. Conclusion

In the present paper, interconnected multi-area power system load frequency control was studied through using a novel optimized fuzzy self-tuning PID controller. In order to improve the proposed control method efficiency, a Tribe-DE optimization algorithm was applied to find the optimal input-output scaling factors and MF parameters of fuzzy PID controllers. Furthermore,

Table 13

Comparative analysis for test system 3.

Controller	ITAE	Settling time (s)					
		Δf_1	Δf_2	Δf_3	$\Delta P_{tie,12}$	$\Delta P_{tie,13}$	$\Delta P_{tie,23}$
Proposed method	2.7771	23.1614	19.8176	24.2801	27.5191	28.0053	24.2411
PID [31]	NR	34.81 (33.46%)	35.56 (44.27%)	32.35 (24.95%)	42.84 (35.76%)	41.67 (32.79%)	38.82 (37.56%)
2DOF IDD [32]	NR	34.10 (32.08%)	28.00 (29.22%)	27.12 (10.47%)	51.64 (46.71%)	62.06 (54.87%)	55.41 (56.25%)
PD-PID Cascade [33]	NR	32.02 (27.67%)	28.34 (30.07%)	NR	30.13 (08.67%)	44.58 (37.18%)	NR

**Fig. 26.** Change in frequency of area 1 after random step load change in area 1 for test system 2 with HVDC link.**Fig. 28.** Change in tie-line power after random step load change in area 1 for test system 2 with HVDC link.**Fig. 27.** Change in frequency of area 2 after random step load change in area 1 for test system 2 with HVDC link.**Fig. 29.** Change in frequency of area 1 after 1% step load increase in area 1 for test system 3.

an error-based on-line rule weight adjustment method was implemented for increasing the robustness of fuzzy PID controllers. The performance of the proposed control method was presented in the regulation purposes of two and three area power systems in parametric uncertainties as well as external disturbance existence. Moreover, the results of damping for frequency and tie-line power flow deviation profiles were compared through

using our proposed method with the methods proposed in references [13,17,21,31,32] and [33]. The proposed control method has the advantages of good transient behavior, less sensitivity to parameter variations and load disturbances as well as the obtained results confirmed the integrity of this approach.

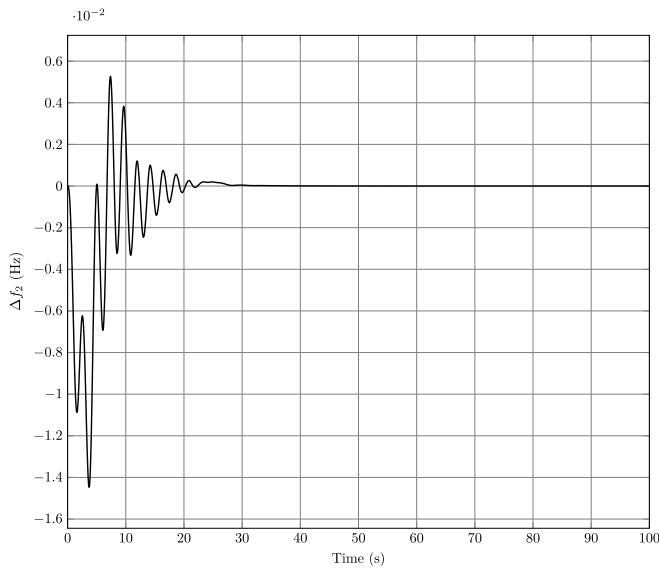


Fig. 30. Change in frequency of area 2 after 1% step load increase in area 1 for test system 3.

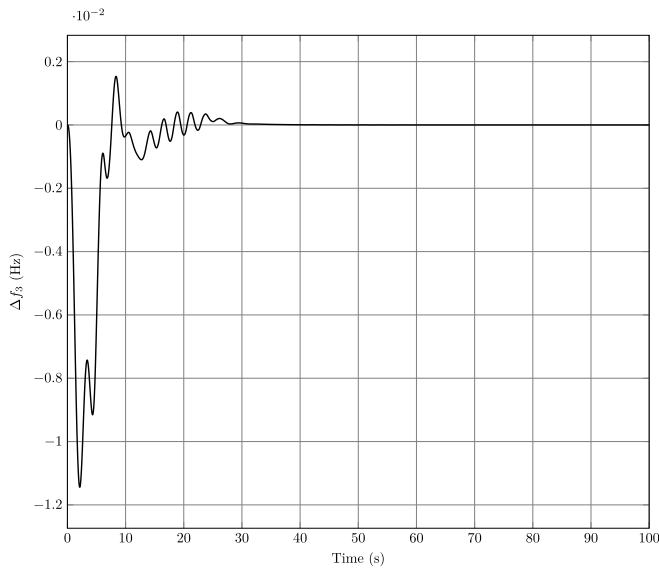


Fig. 31. Change in frequency of area 3 after 1% step load increase in area 1 for test system 3.

In the future, the proposed method shall be tested with complex real-world application such as LFC integrated electric vehicles, wind and photovoltaic systems prior to further confirm its robustness.

CRediT authorship contribution statement

Neda Jalali: Writing-original draft, Resources, Investigation. **Hadi Razmi:** Conceptualization, Methodology, Supervision, Software, Data curation, Formal analysis, Validation. **Hasan Doagou-Mojarrad:** Supervision, Writing-review & editing, Investigation.

Declaration of competing interest

The authors declare that they have no known competing financial interests or personal relationships that could have appeared to influence the work reported in this paper.

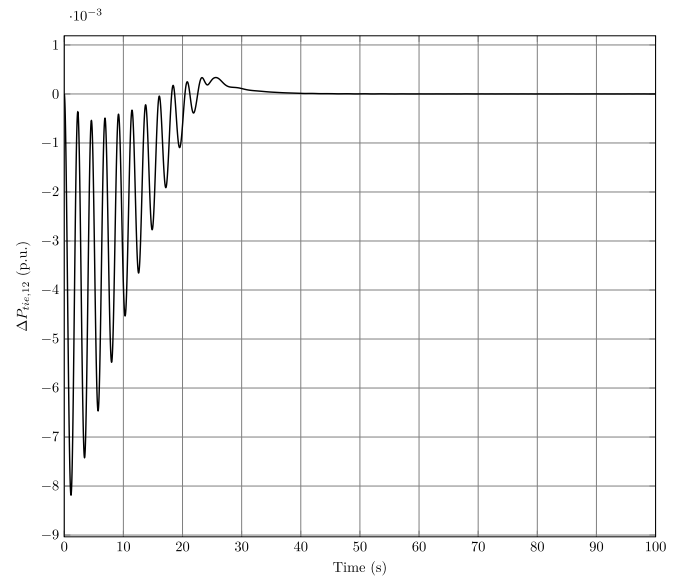


Fig. 32. Change in tie-line power connecting area 1 and area 2 after 1% step load increase in area 1 for test system 3.

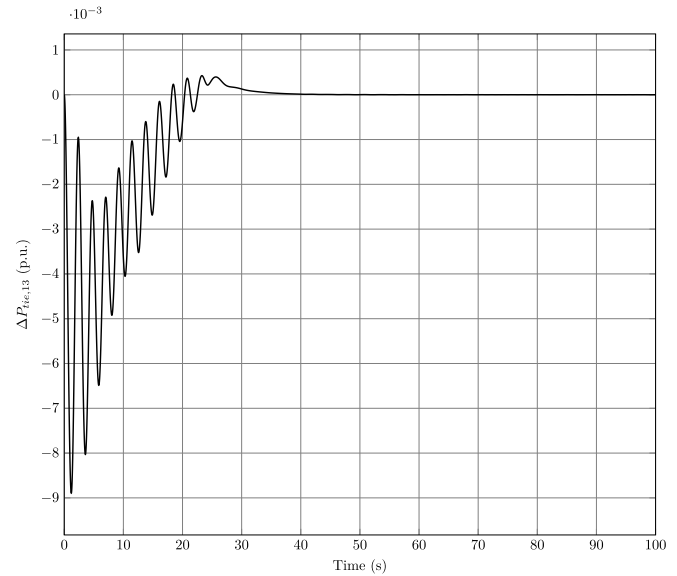


Fig. 33. Change in tie-line power connecting area 1 and area 3 after 1% step load increase in area 1 for test system 3.

Appendix A. Two-area non-reheat thermal power plant [7, 21]

$$B_1 = B_2 = 0.425 \text{ (p.u.MW/Hz)}$$

$$R_{T,1}^{(1)} = R_{T,2}^{(1)} = 2.4 \text{ (Hz/p.u.)}$$

$$T_{GT,1}^{(1)} = T_{GT,2}^{(1)} = 0.08 \text{ (s)}$$

$$T_{TT,1}^{(1)} = T_{TT,2}^{(1)} = 0.3 \text{ (s)}$$

$$K_{T,1}^{(1)} = K_{T,2}^{(1)} = 1$$

$$K_{PS,1} = K_{PS,2} = 120 \text{ (Hz/p.u.)}$$

$$T_{PS,1} = T_{PS,2} = 20 \text{ (Hz/p.u.)}$$

$$T_{12} = 0.545 \text{ (p.u.)}$$

$$\Delta P_{tie} = \Delta P_{tie,1} = -\Delta P_{tie,2}$$

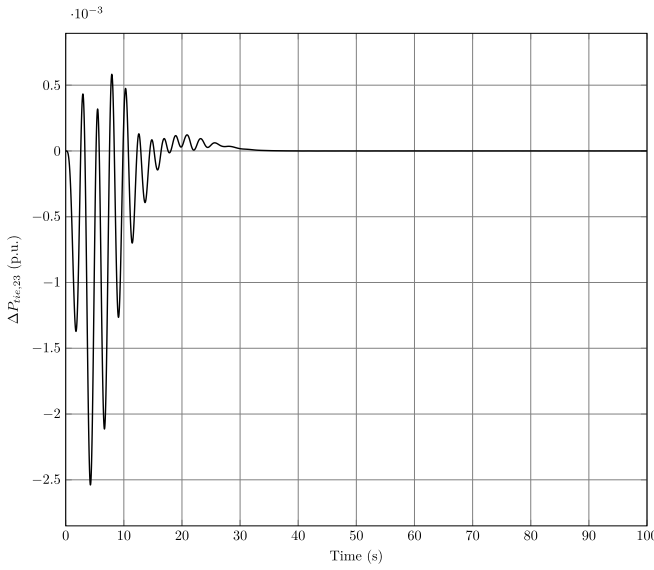


Fig. 34. Change in tie-line power connecting area 2 and area 3 after 1% step load increase in area 1 for test system 3.

Appendix B. Two-area multi-source power plant [30]

$$B_1 = B_2 = 0.4312 \text{ (p.u.MW/Hz)}$$

$$R_{T,1}^{(1)} = R_{T,2}^{(1)} = R_{H,1}^{(1)} = R_{H,2}^{(1)} = R_{G,1}^{(1)} = R_{G,2}^{(1)} = 2.4 \text{ (Hz/p.u.)}$$

$$T_{GT,1}^{(1)} = T_{GT,2}^{(1)} = 0.08 \text{ (s)}$$

$$T_{TT,1}^{(1)} = T_{TT,2}^{(1)} = 0.3 \text{ (s)}$$

$$K_{RT,1}^{(1)} = K_{RT,2}^{(1)} = 0.3$$

$$T_{RT,1}^{(1)} = T_{RT,2}^{(1)} = 10 \text{ (s)}$$

$$K_{PS,1} = K_{PS,2} = 68.9566 \text{ (Hz/p.u.)}$$

$$T_{PS,1} = T_{PS,2} = 11.49 \text{ (Hz/p.u.)}$$

$$T_{12} = 0.0433 \text{ (p.u.)}$$

$$T_{WH,1}^{(1)} = T_{WH,2}^{(1)} = 1 \text{ (s)}$$

$$T_{RH,1}^{(1)} = T_{RH,2}^{(1)} = 5 \text{ (s)}$$

$$T_{DH,1}^{(1)} = T_{DH,2}^{(1)} = 28.75 \text{ (s)}$$

$$T_{GH,1}^{(1)} = T_{GH,2}^{(1)} = 0.2 \text{ (s)}$$

$$C_{VG,1}^{(1)} = C_{VG,2}^{(1)} = 1$$

$$T_{PG,1}^{(1)} = T_{PG,2}^{(1)} = 0.05 \text{ (s)}$$

$$T_{AG,1}^{(1)} = T_{AG,2}^{(1)} = 0.6 \text{ (s)}$$

$$T_{EG,1}^{(1)} = T_{EG,2}^{(1)} = 1 \text{ (s)}$$

$$T_{FG,1}^{(1)} = T_{FG,2}^{(1)} = 0.23 \text{ (s)}$$

$$T_{RG,1}^{(1)} = T_{RG,2}^{(1)} = 0.01 \text{ (s)}$$

$$T_{DG,1}^{(1)} = T_{DG,2}^{(1)} = 0.2 \text{ (s)}$$

$$K_{T,1}^{(1)} = K_{T,2}^{(1)} = 0.543478$$

$$K_{H,1}^{(1)} = K_{H,2}^{(1)} = 0.326084$$

$$K_{G,1}^{(1)} = K_{G,2}^{(1)} = 0.130438$$

$$K_{DC,1} = K_{DC,2} = 1$$

$$T_{DC,1} = T_{DC,2} = 0.2 \text{ (s)}$$

$$\Delta P_{tie} = \Delta P_{tie,1} = -\Delta P_{tie,2}$$

Appendix C. Three-area reheat thermal power plant [31–33]

$$B_1 = B_2 = B_3 = 0.425 \text{ (p.u.MW/Hz)}$$

$$R_{T,1}^{(1)} = R_{T,2}^{(1)} = R_{T,3}^{(1)} = 2.4 \text{ (Hz/p.u.)}$$

$$T_{GT,1}^{(1)} = T_{GT,2}^{(1)} = T_{GT,3}^{(1)} = 0.08 \text{ (s)}$$

$$T_{TT,1}^{(1)} = T_{TT,2}^{(1)} = T_{TT,3}^{(1)} = 0.3 \text{ (s)}$$

$$K_{RT,1}^{(1)} = K_{RT,2}^{(1)} = K_{RT,3}^{(1)} = 0.5$$

$$T_{RT,1}^{(1)} = T_{RT,2}^{(1)} = T_{RT,3}^{(1)} = 10 \text{ (s)}$$

$$K_{PS,1}^{(1)} = K_{PS,2}^{(1)} = K_{PS,3}^{(1)} = 120 \text{ (Hz/p.u.)}$$

$$T_{PS,1} = T_{PS,2} = T_{PS,3} = 20 \text{ (Hz/p.u.)}$$

$$T_{12} = T_{13} = T_{23} = 0.086 \text{ (p.u.)}$$

$$a_{12} = -1/3, a_{13} = -1/6, a_{23} = -1/2$$

$$\Delta P_{tie,1} = \Delta P_{tie,12} + \Delta P_{tie,13}$$

$$\Delta P_{tie,2} = a_{12} \cdot \Delta P_{tie,12} + \Delta P_{tie,23}$$

$$\Delta P_{tie,3} = a_{13} \cdot \Delta P_{tie,13} + a_{23} \cdot \Delta P_{tie,23}$$

$$\dot{\Delta P}_{tie,12} = 2\pi T_{12}(\Delta f_1 - \Delta f_2)$$

$$\dot{\Delta P}_{tie,13} = 2\pi T_{13}(\Delta f_1 - \Delta f_3)$$

$$\dot{\Delta P}_{tie,23} = 2\pi T_{23}(\Delta f_2 - \Delta f_3)$$

References

- [1] H. Shayeghi, H. Shayanfar, A. Jalili, Load frequency control strategies: A state-of-the-art survey for the researcher, *Energy Convers. Manage.* 50 (2) (2009) 344–353.
- [2] A. Pappachen, A.P. Fathima, Load frequency control in deregulated power system integrated with SMES-TCPS combination using ANFIS controller, *Int. J. Electr. Power Energy Syst.* 82 (2016) 519–534.
- [3] S. Saxena, Load frequency control strategy via fractional-order controller and reduced-order modeling, *Int. J. Electr. Power Energy Syst.* 104 (2019) 603–614.
- [4] A. Kosari, H. Jahanshahi, S. Razavi, An optimal fuzzy PID control approach for docking maneuver of two spacecraft: Orientational motion, *Eng. Sci. Technol.* 20 (1) (2017) 293–309.
- [5] E. Nikmanesh, O. Hariri, H. Shams, M. Fasihozaman, Pareto design of load frequency control for interconnected power systems based on multi-objective uniform diversity genetic algorithm (MUGA), *Int. J. Electr. Power Energy Syst.* 80 (2016) 333–346.
- [6] M.H. Amoozgar, A. Chamseddine, Y. Zhang, Fault-tolerant fuzzy gain-scheduled PID for a quadrotor helicopter testbed in the presence of actuator faults, *IFAC Proc. Vol.* 45 (3) (2012) 282–287.
- [7] R.K. Sahu, S. Panda, A. Biswal, G.C. Sekhar, Design and analysis of tilt integral derivative controller with filter for load frequency control of multi-area interconnected power systems, *ISA Trans.* 61 (2016) 251–264.
- [8] E. Ali, S. Abd-Elazim, BFOA based design of PID controller for two area load frequency control with nonlinearities, *Int. J. Electr. Power Energy Syst.* 51 (2013) 224–231.
- [9] S. Padhan, R.K. Sahu, S. Panda, Application of firefly algorithm for load frequency control of multi-area interconnected power system, *Electric Power Compon. Syst.* 42 (13) (2014) 1419–1430.
- [10] R.K. Sahu, S. Panda, U.K. Rout, D.K. Sahoo, Teaching learning based optimization algorithm for automatic generation control of power system using 2-DOF PID controller, *Int. J. Electr. Power Energy Syst.* 77 (2016) 287–301.
- [11] C.K. Shiva, V. Mukherjee, A novel quasi-oppositional harmony search algorithm for automatic generation control of power system, *Appl. Soft Comput.* 35 (2015) 749–765.
- [12] C.K. Shiva, V. Mukherjee, A novel quasi-oppositional harmony search algorithm for AGC optimization of three-area multi-unit power system after deregulation, *Eng. Sci. Technol.* 19 (1) (2016) 395–420.

- [13] M. Gheisarnejad, An effective hybrid harmony search and cuckoo optimization algorithm based fuzzy PID controller for load frequency control, *Appl. Soft Comput.* 65 (2018) 121–138.
- [14] M.Z. Bernard, T.H. Mohamed, Y.S. Qudaih, Y. Mitani, Decentralized load frequency control in an interconnected power system using coefficient diagram method, *Int. J. Electr. Power Energy Syst.* 63 (2014) 165–172.
- [15] Y. Zhao, E.G. Collins, Fuzzy PI control design for an industrial weigh belt feeder, *IEEE Trans. Fuzzy Syst.* 11 (3) (2003) 311–319.
- [16] M. Güzelkaya, I. Eksin, E. Yeşil, Self-tuning of PID-type fuzzy logic controller coefficients via relative rate observer, *Eng. Appl. Artif. Intell.* 16 (3) (2003) 227–236.
- [17] Y. Arya, N. Kumar, Design and analysis of BFOA-optimized fuzzy PI/PID controller for AGC of multi-area traditional/restructured electrical power systems, *Soft Comput.* 21 (21) (2017) 6435–6452.
- [18] D.K. Sahoo, R.K. Sahu, G.C. Sekhar, S. Panda, A novel modified differential evolution algorithm optimized fuzzy proportional integral derivative controller for load frequency control with thyristor controlled series compensator, *J. Electr. Syst. Inf. Technol.* 5 (3) (2018) 944–963.
- [19] A. Zamani, S.M. Barakati, S. Yousofi-Darmian, Design of a fractional order PID controller using GBMO algorithm for load-frequency control with governor saturation consideration, *ISA Trans.* 64 (2016) 56–66.
- [20] B.K. Sahu, T.K. Pati, J.R. Nayak, S. Panda, S.K. Kar, A novel hybrid LUS-TLBO optimized fuzzy-PID controller for load frequency control of multi-source power system, *Int. J. Electr. Power Energy Syst.* 74 (2016) 58–69.
- [21] R.K. Sahu, S. Panda, G.T.C. Sekhar, A novel hybrid PSO-PS optimized fuzzy PI controller for AGC in multi area interconnected power systems, *Int. J. Electr. Power Energy Syst.* 64 (2015) 880–893.
- [22] D. Tripathy, A.K. Barik, N.B.D. Choudhury, B.K. Sahu, Performance comparison of SMO-based fuzzy PID controller for load frequency control, in: *Soft Computing for Problem Solving*, Springer, 2019, pp. 879–892.
- [23] M. Yang, C. Li, Z. Cai, J. Guan, Differential evolution with auto-enhanced population diversity, *IEEE Trans. Cybern.* 45 (2) (2014) 302–315.
- [24] O. Karasakal, M. Guzelkaya, I. Eksin, E. Yesil, An error-based on-line rule weight adjustment method for fuzzy PID controllers, *Expert Syst. Appl.* 38 (8) (2011) 10124–10132.
- [25] Y. Zheng, J. Zhou, Y. Xu, Y. Zhang, Z. Qian, A distributed model predictive control based load frequency control scheme for multi-area interconnected power system using discrete-time Laguerre functions, *ISA Trans.* 68 (2017) 127–140.
- [26] C. Ramlal, A. Singh, S. Rocke, M. Sutherland, Decentralized fuzzy H_∞ -iterative learning LFC with time-varying communication delays and parametric uncertainties, *IEEE Trans. Power Syst.* (2019).
- [27] M. Shiroei, A. Ranjbar, Supervisory predictive control of power system load frequency control, *Int. J. Electr. Power Energy Syst.* 61 (2014) 70–80.
- [28] R. Storn, K. Price, Differential evolution—a simple and efficient heuristic for global optimization over continuous spaces, *J. Global Optim.* 11 (4) (1997) 341–359.
- [29] H. Razmi, H. Doagou-Mojarrad, Comparative assessment of two different modes multi-objective optimal power management of micro-grid: grid-connected and stand-alone, *IET Renew. Power Gener.* 13 (6) (2018) 802–815.
- [30] B. Mohanty, S. Panda, P. Hota, Controller parameters tuning of differential evolution algorithm and its application to load frequency control of multi-source power system, *Int. J. Electr. Power Energy Syst.* 54 (2014) 77–85.
- [31] Y. Sharma, L.C. Saikia, Automatic generation control of a multi-area ST-Thermal power system using grey wolf optimizer algorithm based classical controllers, *Int. J. Electr. Power Energy Syst.* 73 (2015) 853–862.
- [32] P. Dash, L.C. Saikia, N. Sinha, Comparison of performances of several cuckoo search algorithm based 2DOF controllers in AGC of multi-area thermal system, *Int. J. Electr. Power Energy Syst.* 55 (2014) 429–436.
- [33] P. Dash, L.C. Saikia, N. Sinha, Automatic generation control of multi area thermal system using bat algorithm optimized PD-PID cascade controller, *Int. J. Electr. Power Energy Syst.* 68 (2015) 364–372.